Manipulation of Flexible Structural Modules by Space Robots During LSS Construction

by

Dimitrios Spyridon Tzeranis

Diploma, Mechanical Engineering
National Technical University of Athens, 2003

Submitted to the Department of Mechanical Engineering
in Partial Fulfillment of the Requirements for the Degree of
Master of Science in Mechanical Engineering

at the

Massachusetts Institute of Technology

September 2005

Signature of Author .....
Department of Mechanical Engineering
August 15, 2005

Certified by .....
Steven Dubowsky
Professor of Mechanical Engineering
Thesis Supervisor

Accepted by .....
Professor Lallit Anand
Chairman, Committee on Graduate Students

Manipulation of Flexible Structural Modules by Space Robots During LSS Construction

by

Dimitrios Spyridon Tzeranis

Submitted to the Department of Mechanical Engineering
on August 15, 2005 in Partial Fulfillment of the
Requirements for the Degree of Master of Science in
Mechanical Engineering

ABSTRACT

Future space structures are expected to have very large size. Such Large Space Structures (LSS) will be constructed in-orbit, probably by assembling large structural modules. This is a dangerous and difficult task for humans. On the other hand, this is a challenging and promising application for space robotics.

This work provides a planning and control architecture for the manipulation of a large flexible structural module in the proximity of the LSS, by a team of space manipulators that are mounted on the LSS. In this task, the payload (module) and the base structure (LSS) of the robots are assumed to be very compliant. Interface forces between robots and flexible structures induce undesirable vibration. The approach developed here is to plan and control the forces that robots apply to the flexible structures so that they maneuver the module precisely while exciting low levels of residual vibration in the module and the LSS. Robot use different control implementations to control the forces they apply to different kinds of flexible structures. Robots plan and control cooperatively the forces they apply to the module. Each robot exploits its redundancy to minimize the base reaction forces it applies to the LSS and to avoid undesirable configurations.

Simulation results demonstrate the effectiveness of the developed architecture in positioning the module precisely and exciting low levels of residual vibration in the module and the LSS.

Thesis Supervisor: Steven Dubowsky

Title: Professor of Mechanical Engineering

Acknowledgements

I would like to thank Professor Steven Dubowsky for his guidance, his patience and for giving me the chance to be a member of the MIT Field and Space Robotics Laboratory.

I would also like to thank the students and faculty of the Field and Space Robotics Laboratory for their support and for making my staying in the lab more enjoyable. Special thanks to Dr. Matt Lichter, Mrs Peggy Boning, Mr. Vickram Mangalgiri, Mr. Shingo Shimoda, Dr. Sauro Liberatore, Mr. Hiroshi Ueno, Mr. Yoshiyuki Ishijima, Prof. Yoji Kuroda, Miss Amy Bilton, Mr. J. S. Plante and Mr. Steve Peters.

I would like to thank my friends at MIT for making Boston winters feel less dark. Finally, I would like to thank my parents, my brother and my friends back in Greece for their endless love, their delicious cookies and the inspiration they provide to me.

This work was supported by the Japanese Aerospace Exploration Agency (JAXA).

ΤΡΕΙΣ ΨΥΧΕΣ, ΤΡΕΙΣ ΠΡΟΣΕΥΧΕΣ:
Α' ΔΟΞΑΡΙ ΕΙΜΑΙ ΣΤΑ ΧΕΡΙΑ ΣΟΥ, ΚΥΡΙΕ, ΤΕΝΤΩΣΕ ΜΕ, ΑΛΛΙΩΣ ΘΑ ΣΑΠΙΣΩ.
Β' ΜΗ ΜΕ ΠΑΡΑΤΕΝΤΩΣΕΙΣ, ΚΥΡΙΕ, ΘΑ ΣΠΑΣΩ.
Γ' ΠΑΡΑΤΕΝΤΩΣΕ ΜΕ, ΚΥΡΙΕ, ΚΙ ΑΣ ΣΠΑΣΩ !

Νίκος Καζαντζάκης, Αναφορά στον Γκρέκο

Table of Contents

List of Figures

List of Tables

Notation

$\underline{A}_F$	System matrix of the linearized robots-module dynamics
$\underline{A}_F^*$	System matrix of the modified linearized robots-module dynamics
$\underline{A}_p$	Coefficient matrix used in force planning
$\underline{B}_{Ai}$	Mass matrix of robot i (with respect to its operational space) [kg]
$\underline{B}_F$	Input matrix of the linearized robots-module dynamics
$\underline{B}_i$	Mass matrix of robot i (with respect to its joint space) [kgm^2]
$\underline{B}_p$	Vector used in force planning
$\underline{C}_F$	Output matrix of the linearized robots-module dynamics
$\underline{D}_{Ai}$	Damping matrix of robot i (with respect to its operational space) [Nsec/m]
$\underline{D}_{Aid}$	Desired active damping matrix for robot i (with respect to its operational space) [Nsec/m]
$\underline{f}_{bi}$	Base reaction force of robot i [N]
$\underline{\tilde{f}}_{bi}$	Tracking error of $\underline{f}_{bi}$ [N]
$\underline{f}_{bid}$	Desired base reaction force of robot i [N]
f_i	Frequency of beam's mode i [Hz]
$\underline{f}_{si}$	Force applied to the module by robot i [N]
$\underline{F}_{si}$	Laplace transformation of $\underline{f}_{si}$ [N]
$\underline{\tilde{f}}_{si}$	Tracking error of $\underline{f}_{si}$ [N]
f_{sij}	The j component (j = X, Y) of $\underline{f}_{si}$ [N]
$\underline{f}_{sid}$	Desired force $\underline{f}_{si}$ to be applied by robot i to the module [N]
$\underline{F}_{sid}$	Laplace transformation of $\underline{f}_{sid}$ [N]
f_{sijd}	The j component (j = X, Y) of $\underline{f}_{sid}$ [N]
$\underline{G}_{BF}$	Transfer matrix for the PI controllers of the base reaction force/moment controller
$\underline{G}_F$	Transfer matrix of the linearized robots-module dynamics
$\underline{G}_F^{-1}$	Transfer matrix of the inverse linearized robots-module dynamics
G_{FCj}	PI controller for the j component (j = X, Y) of $\underline{\tilde{f}}_{si}$ (part of the endpoint force controller)
$\underline{H}_i$	Angular momentum of robot i with respect to its center of mass [kg·m^2/sec]
h_i	Excitation function of beam's mode i [N]
hsv_i	Hankel singular value for the beam's mode i
$\underline{J}_{ei}$	Jacobian matrix for expressing $\underline{\dot{r}}_{ei}$ with respect to $\underline{\theta}_i$ [m/rad]
$\underline{J}_{Gi}$	Jacobian matrix for expressing $\underline{\dot{r}}_{Gi}$ with respect to $\underline{\dot{\vartheta}}_i$ [m/rad]
$\underline{J}_{Ri}$	Jacobian matrix for expressing the momentum of robot i as a function of $\underline{\dot{\vartheta}}_i$

$\underline{\hat{J}}_{Ri}$	Computationally efficient approximation of $\underline{J}_{Ri}$
$\underline{J}_{tei}$	Jacobian matrix for expressing $\dot{\underline{r}}_{ei}$ with respect to $\dot{\underline{\vartheta}}_i$ [m/rad]
k_B	Spring rate used to model the dynamics of the base structure of each robot [N/m]
K_{Ij}	I term of the G_{FCj} controller
K_F	State feedback gain used in the endpoint force controller
K_{Pj}	P term of the G_{FCj} controller
$\underline{L}_i$	Linear momentum of robot i [kg·m/sec]
M	Number of sinusoids used to express each component of f_{sijd}
m_B	Mass used to model the dynamics of the base structure of each robot [kg]
m_{Ri}	Robot i mass [kg]
$\underline{\underline{M}}_{sr}$	Beam mass matrix (rigid body motion)
Q	Number of assumed modes used to describe beam vibration
$\underline{q}_s$	Beam modal coefficient vector
q_{si}	The i-th modal coefficient of the beam
$\underline{r}_{ei}$	Position of robot i end-effector with respect to its base [m]
$\hat{\underline{r}}_{ei}$	Estimated $\underline{r}_{ei}$ [m]
$\underline{r}_{Gei}$	Position of robot i end-effector with respect to its CM [m]
$\underline{r}_{Gi}$	Position of robot i CM with respect to its base [m]
$\underline{r}_{Gs}$	Position of the beam CM with respect to the origin of the inertial frame XYZ [m]
s_i	Pole of beam mode i (free-free)
u	Beam vibration displacement in the y_m direction at x_m [m]
$\underline{\underline{U}}$	Matrix whose columns are the principal axes of inertia of $\underline{B}_{Ai}$
$\underline{\underline{W}}_{sr}$	Grasp matrix for the beam rigid body motion
$\underline{\underline{W}}_{sv}$	Grasp matrix for the beam vibration motion
XYZ	Inertial coordinate system axes
$\underline{x}_F$	State vector of the linearized robots-module dynamics
$X_m Y_m Z_m$	Body-fixed coordinate system axes attached at the beam CM
$\underline{x}_s$	Beam generalized coordinates
$\underline{x}_{sr}$	Beam rigid body coordinates
y_{bi}	Vibration displacement of the robot i base [m]
$\underline{a}$	Vector containing all a_{ijk}
a_{ijk}	Parameters used to express f_{sijd} as a sum of sinusoids
$\underline{\gamma}_i$	Contribution of the end-effector forces due to joint actuation $\underline{\tau}_i$ [N]
$\underline{\gamma}_{Ei}$	Contribution of the endpoint forces $\underline{f}_{si}$ due to joint actuation $\underline{\tau}_{Ei}$ [N]
${}^C\underline{\gamma}_{Ei}$	Contribution of the endpoint forces $\underline{f}_{si}$ due to joint actuation ${}^C\underline{\tau}_{Ei}$ [N]

$^{C}\underline{\Gamma}_{Ei}$	Laplace transformation of $^{C}\underline{\gamma}_{Ei}$
$^{D}\underline{\gamma}_{Ei}$	Contribution of the endpoint forces $\underline{f}_{si}$ due to joint actuation $^{D}\underline{\tau}_{Ei}$ [N]
$^{F}\underline{\gamma}_{Ei}$	Contribution of the endpoint forces $\underline{f}_{si}$ due to joint actuation $^{F}\underline{\tau}_{Ei}$ [N]
$\delta\underline{r}_{Gs}$	Maximum allowable positioning error for the beam CM $\underline{r}_{Gs}$ [m].
δu_{tip}	Maximum allowable residual vibration in the beam ends [m]
δy_{bi}	Maximum allowable residual vibration in the robot base structures [m]
$\delta\theta_s$	Maximum allowable positioning error of the beam orientation θ_s [rad]
Δt	Maneuver duration [sec]
ζ_i	Damping ratio of beam mode i
$\underline{Z}_s$	Beam modal matrix
$\underline{\eta}_{Ai}$	Nonlinear forces of robot i (with respect to its operational space) [N]
$\underline{\eta}_i$	Nonlinear and friction forces of robot i (with respect to its joint space) [Nm]
$\underline{\eta}_i^*$	Nonlinear and friction forces of the "robot i and base structure" system (with respect to its joint space)
$\underline{\theta}_i$	Joint angle vector of robot i [rad]
$\underline{\theta}_{id}$	Desired joint angle vector of robot i [rad]
θ_{ij}	The j-th joint angle of robot i [rad]
θ_s	Orientation of the beam neutral axis [rad]
$\underline{\vartheta}_i$	Generalized coordinates of robot i (including reaction wheels) [rad]
$\underline{\mu}_{bi}$	Base reaction moments of robot i [Nm]
$\underline{\tilde{\mu}}_{bi}$	Tracking error of $\underline{\mu}_{bi}$ [N]
$\underline{\mu}_{bid}$	Desired base reaction moments of robot i [Nm]
$\mu_{\max}$	Maximum eigenvalue of the inertia matrix $\underline{B}_{Ai}$ [kg]
$\mu_{\min}$	Minimum eigenvalue of the inertia matrix $\underline{B}_{Ai}$ [kg]
$\sigma(\cdot)$	Singular values of a square matrix
$\underline{\tau}_{Bi}$	Joint torque output of the base reaction force/moment controller of robot i [Nm]
$\tau_{damp,i}$	Joint torque applied in robot i to generate the desired damping matrix $\underline{D}_{Aid}$ [Nm]
$\underline{\tau}_{Ei}$	Joint torque output of the endpoint force controller for robot i [Nm]
$^{C}\underline{\tau}_{Ei}$	The part of $\underline{\tau}_{Ei}$ from the centralized part of the endpoint force controller [Nm]
$^{D}\underline{\tau}_{Ei}$	The part of $\underline{\tau}_{Ei}$ from the decentralized part of the endpoint force controller [Nm]
$^{F}\underline{\tau}_{Ei}$	Feed-forward action of the endpoint force controller [Nm]
$\underline{\tau}_i$	Joint torque vector of robot i [Nm]
$\underline{\tau}_{Mi}$	Joint torque output of robot i motion controller [Nm]
$^{C}\underline{\tau}_{Mi}$	The part of $\underline{\tau}_{Mi}$ from the joint PD controllers of robot i [Nm]

$\underline{\tau}_{Mi}^{F}$	Feed-forward action in the robot motion controller [Nm]
$\underline{\phi}(x_s)$	$Q \times 1$ vector that contains $\phi_i(x_s)$, i = 1, ..., Q
$\phi_i(x_s)$	The i-th assumed mode of the beam evaluated at x_s
ψ_i	Angular position of the reaction wheel of robot i [rad]
ψ_{id}	Desired angular position of the reaction wheel of robot i [rad]
ω	Angular frequency [rad/sec]
ω_C	Cut-off frequency of the low-pass filter used to avoid spillover in the endpoint force controller [rad/sec]
ω_{Fbw}	Bandwidth of the robot endpoint force controller [rad/sec]
ω_i	Natural frequency of beam mode i [rad/sec]
ω_{pi}	Natural frequency of the sinusoids used to express f_{sijd} [rad/sec]
$\underline{\Omega}_s$	Beam natural frequency matrix [rad/sec]

All position and force vectors are expressed with respect to the inertial frame XYZ, except from the vibration displacement $u(x_m)$ with is expressed with respect to the body-fixed coordinate system $X_m Y_m Z_m$ (see Fig. 2.4).

Chapter 1
Introduction

1.1 Introduction

This thesis presents a planning and control architecture for the cooperative manipulation of a large flexible space structure by a team of robot manipulators mounted on a Large Space Structure (LSS). This work took place at the MIT Field and Space Robotics Laboratory and is the author's contribution to the joint MIT – JAXA research project on the study of space robotic systems.

One major potential application of space robots is the construction of Large Space Structures. This task requires robots to maneuver delicate structures, which will probably have large size and flexibility. Interaction forces between robots and structures induce vibration that damps slowly, delay the construction progress, and can damage the structures and the robots. The robot planning and control architecture described in this thesis exploits robot redundancy and cooperation to enhance their ability to interact with flexible structures of large size without inducing significant residual vibration or excessive forces.

1.2 Motivation

There is significant international interest in building Space Solar Power Stations (SSPS) within the next twenty to fifty years [27]. SSPS will use large mirrors (on the

order of kilometers in size) to collect solar radiation. This power will be transformed into electrical power and then transmitted to earth by microwaves or laser beams, Fig 1.1.

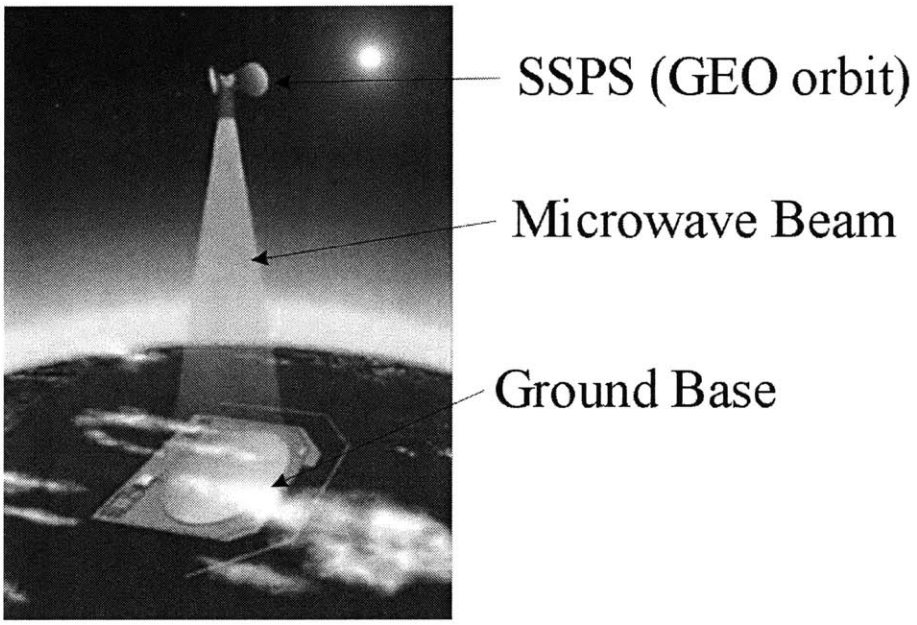

Figure 1.1. Concept for the proposed Space Solar Power System of JAXA [50].

Future space structures, such as SSPS and orbital telescopes, will be considerably larger compared to existing space structures like the International Space Station (ISS) [22]. The construction of such structures by human extra-vehicular activity (EVA) will be too expensive and dangerous. The use of robots is a promising alternative.

The robotic construction of LSS is assumed to take place in two steps, Fig 1.2. The first step is the transportation of raw material in orbit and the construction of large structural sub-assemblies (on the order of 100-200 m) by assembling small structural elements (e.g. rods) [9]. These sub-assemblies are transported in the proximity (about 10 m) of the LSS under construction by a team of free-flying robots [17]. In the second step, each module is manipulated into its pre-assembly position and assembled with the LSS by robot manipulators mounted on the LSS.

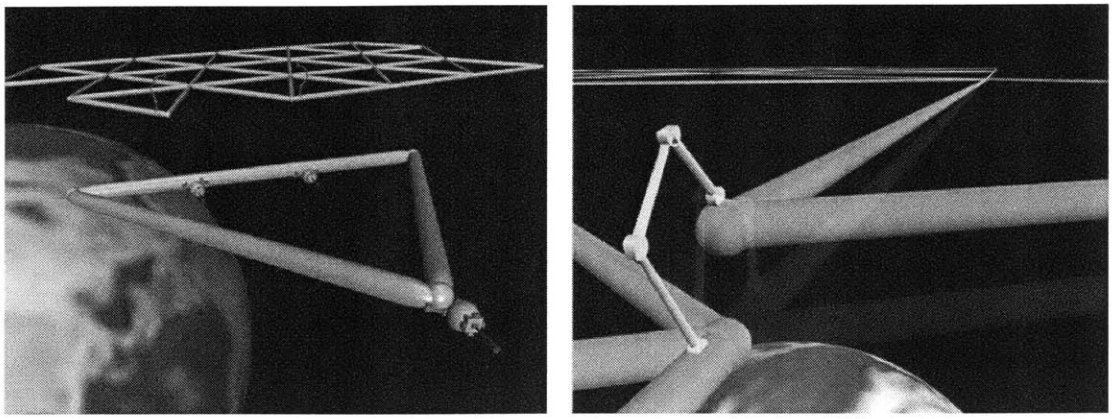

Transportation of LSS modules in the proximity of the LSS

Assembly the LSS modules with the LSS

Figure 1.2. Steps in the robotic construction of Large Space Structures.

At the moment, new robotic manipulators (the European Robotic Arm (ERA) and the Japan Experiment Module Remote Manipulator (JEMRMS)) are planned to be installed in the ISS to assist astronauts in construction and maintenance tasks [20, 49, 50], Fig 1.3. However, the necessary dexterity skills for robots to accomplish LSS construction tasks are beyond today's state of the art.

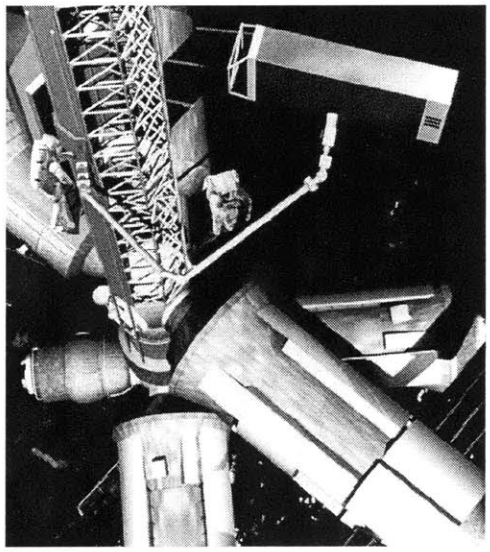

Figure 1.3. Schematic of astronauts using the European Robotic Arm to install a solar array [49].

1.3 Problem Statement

This study focuses on the last phase of LSS construction, Fig 1.2, in which a large flexible structural module of the LSS has just been transported in the proximity of its pre-assembly position [17]. The module is grasped by a team of robot manipulators, which are mounted on the LSS. The robots must manipulate the module into its pre-assembly position, where the two structures will be connected probably by self-latching mechanisms [10].

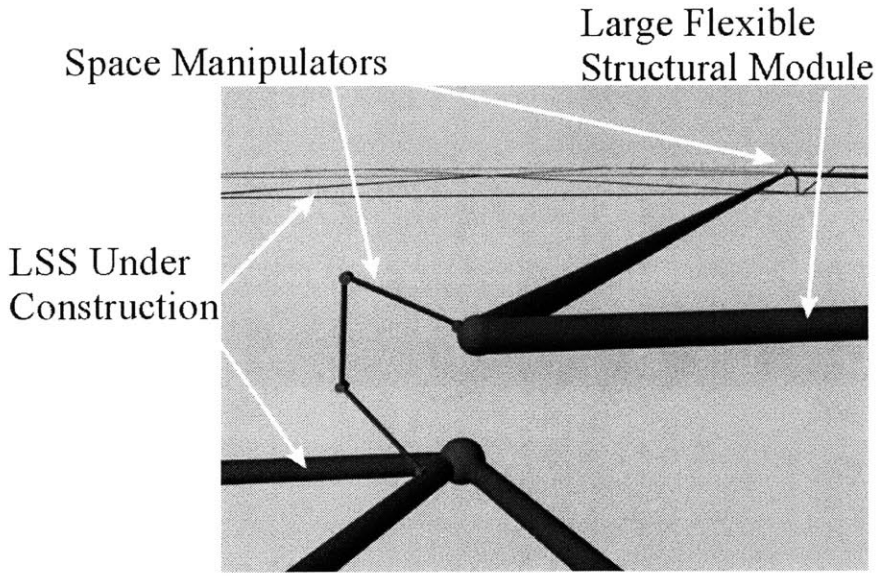

Figure 1.4. Schematic of a large flexible structural module of the LSS that is manipulated by a team of robots based on the LSS.

During this manipulation task, robots interact with space structures (the module and the LSS), which are extremely lightweight and compliant. Forces applied by robots to such structures can induce large deflections and vibration, which damps very slowly due to the poor damping of space structures [12]. Residual vibration in the module or the LSS prevents latching mechanisms from operating. This induces costly time delays. Residual vibration can also cause collisions that could damage the space structures and

the robots. For these reasons, robots should manipulate the structural module precisely while inducing low levels of residual vibration in the module and their base structures.

The cooperative manipulation of LSS modules is a challenging task for the robots involved. Space robots have limited actuation and lightweight designs, Fig. 1.5. They are susceptible to damage from large forces applied to their end-effectors or when they reach their joint limits. Vibration in the robots' base structures (here the LSS) can degrade the performance of their controllers or force them into undesirable configurations.

Robot cooperation is an important aspect of this task. A single robot will probably not be able to position such a large structure reliably. On the other hand, a team of robots can distribute loads to keep the required joint torques within their actuator limits, and exchange sensory information to acquire a better estimate of the system's state.

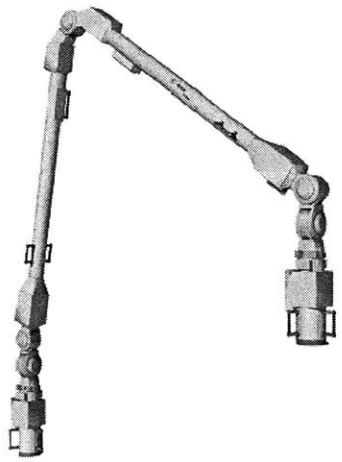

Figure 1.5. The European Robotic Arm [49].

1.4 Background and Literature Review

On-orbit construction of space structures has been an area of research for more than thirty years. The main motivation has been the construction of space solar power

systems and orbital telescopes [20, 27]. Studies show that the construction of LSS by human EVA will be impractical and dangerous [44]. Many studies focus on using simple machines or robots to construct space structures by assembling simple structural elements such are rods and beams [9, 10, 20, 30, 36, 44]. However, it is believed that future LSS will probably be constructed by assembling large structural sub-assemblies, which will be assembled in orbit [9, 22]. Some studies focus on the design of the elementary structural elements of LSS and the latching mechanisms that are used to connect them during assembly [10, 44].

The robotic construction of LSS has been studied mainly during the last decade. Some studies focus on using robots to progressively build truss structures by assembling rods [10, 30]. The use of existing space robot facilities to construct space structures is analyzed in [20]. Robots of various kinds are considered to participate in various tasks of the LSS construction [45], Fig 1.6. These include free-flying robots that transport structural modules [17], free-flying robots that provide sensory information [21, 45], robot manipulators that walk on the surface of the LSS to perform tasks at various locations [35, 42] and tele-operated robots [14, 45]. High level planning of the robotic assembly of LSS that considers structural dimensional mismatch is addressed in [22]. In the large majority of these studies, robot size is comparable with the size of the structural elements that are assembled.

LSS control schemes focus mainly in designing robust stable state-feedback controllers to damp vibration that is induced in the LSS by external disturbances [2, 3, 12, 16]. The proposed algorithms control a large number of modes by using on-board sensors (rate sensors and accelerometers) and usually embedded piezoelectric actuators.

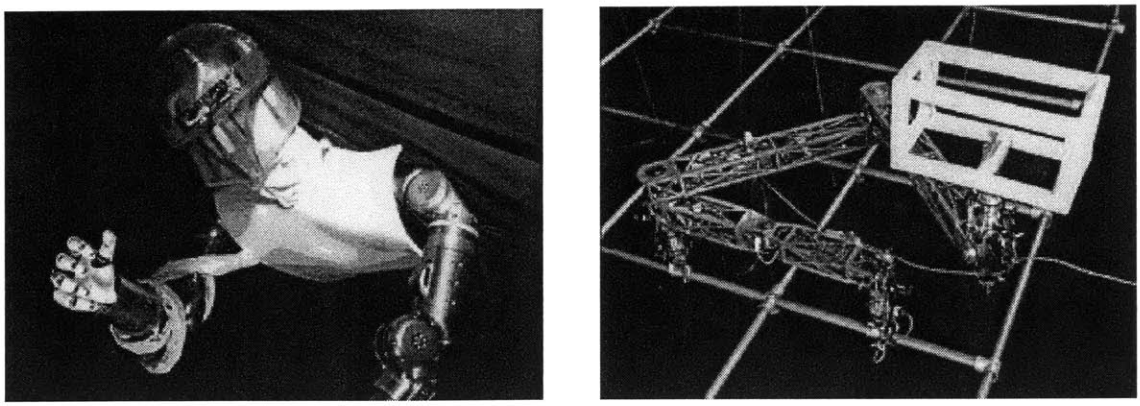

Figure 1.6. Robot concepts for LSS assembly. a) Robonaut tele-operated robot, b) Skyworker walking robot, [45].

There is a significant amount of work in the area of planning time or fuel optimal maneuvers for flexible structures or spacecrafts [5, 24, 33, 41]. Structural flexibility is usually modeled through the finite element method [11]. Optimization techniques provide analytical solutions for optimum one-dimensional point-to-point motions [6]. Optimization problems in three dimensions are solved numerically [11]. Studies in flexible spacecraft maneuvering model the actuators as point forces, which is a good approximation for thrusters. However, when the structure is maneuvered by robot manipulators, the analysis should consider their dynamics and kinematics.

An important aspect of maneuvering flexible structures is the minimization of residual vibration that is induced by actuation. A popular approach is the pre-shaping of input commands [32, 34]. A somewhat more general approach is presented in [6].

This thesis considers the cooperative manipulation of a large flexible space structure by a team of robots. The mechanics of cooperative robotic manipulation are described in [26]. Proposed control algorithms for the cooperative manipulation of rigid objects include joint space controllers [7], impedance controllers [25], and adaptive

controllers [43]. There are also a number of studies on the planning and control of robots that manipulate flexible objects [37, 38, 39, 48]. These studies consider cases where the flexible object is smaller than the robots, usually pieces of sheet metal that need to be deformed before their assembly.

Various research groups have studied the problem of planning the motion of a robot mounted on a compliant structure so that the vibration excitation in the compliant base structure is minimized [40, 46]. These approaches require some knowledge of the robot base structure dynamics. This probably will not be the case in LSS assembly, where each robot will operate at various locations of the LSS and will probably have limited knowledge of the dynamics of its supporting structure.

To date, there are no studies on the planning and control of a team of robots, which are mounted on compliant base structures, so that they manipulate a large flexible structure (an order of magnitude larger than the robots) and induce low levels of residual vibration in the flexible structure and their base structures. This problem is addressed in this thesis.

1.5 Contributions of this Thesis

This thesis presents a planning and control architecture for the manipulation of a large flexible space structural module by a team of redundant robot manipulators, which are mounted on rigid or compliant base structures. The objective is to manipulate the module into its pre-assembly position precisely and to excite low residual vibration in the module and the compliant base structures of the robots.

The main idea of the developed architecture is to plan and control the interaction forces between the robots and the flexible space structures. The desired interaction forces are planned so that when applied to the flexible structures, they result in desired system response (in terms of positioning accuracy and residual vibration). Robots use force/torque sensors to measure and control these interaction forces. The control of the forces that robots apply to the module is improved by exploiting robot cooperation and proper redundant robot designs. Each robot also exploits its redundancy to control the forces it applies to the LSS, and to avoid undesirable configurations.

1.6 Thesis Outline

The developed architecture for the cooperative manipulation of large flexible structural modules is described in the next two chapters, following this introduction. Chapter 2 provides a more detailed description of the task, describes the developed planning and control architecture when robots are assumed to be mounted on a rigid base structure, and provides simulation results. Chapter 3 extends the architecture to the case where robots are mounted on compliant base structures, and provides simulation results. Chapter 4 summarizes this study and provides ideas for future research. The appendices contain background material. Appendix A provides the derivation of the linearized system dynamics that are used to design the force controller algorithms of Chapters 2 and 3. Appendix B provides preliminary design specifications for experiments that will validate the planning and control architecture developed in this study.

Chapter 2
Manipulation of Large Flexible Structures by Robots Mounted on Rigid Bases

2.1 Introduction

The precision manipulation of large structural modules in the close proximity of LSS is a challenging task that space robots will face during the construction of Large Space Structures. This task will probably not be accomplished by a single robot due to actuation limitations and safety concerns. It will require a team of cooperative robots that will be able to interact with structures of significant size and flexibility.

This chapter describes a planning and control architecture for the manipulation of a large flexible module by a team of robots. Here, the robots are assumed to be mounted on a rigid structure. Compliant base structures will be discussed in Chapter 3. In the developed architecture, robots plan and control cooperatively the forces that they apply to the module. Each robot controls also the motion of its redundant degrees of freedom to avoid collisions and undesirable configurations.

This chapter starts by providing a more detailed description of the manipulation task. It presents the developed planning and control architecture and provides simulation results to demonstrate its effectiveness in positioning the module accurately and with low levels of residual vibration.

2.2 Task Description

Fig. 2.1 shows a representative manipulation task. A large flexible structural module of the LSS (about 200m) has been transported in the proximity of the LSS (about 10 m from the LSS), near its pre-assembly position, by free-flying robots [17]. A team of robot manipulators have already firmly grasped the module at proper grasping points. The robots must maneuver the module into its pre-assembly position (about 1m from the LSS), where it will be assembled with the LSS. The robot manipulators are mounted on the LSS. In this chapter, the compliance of the LSS is neglected and the robots are assumed to be mounted on a rigid base structure.

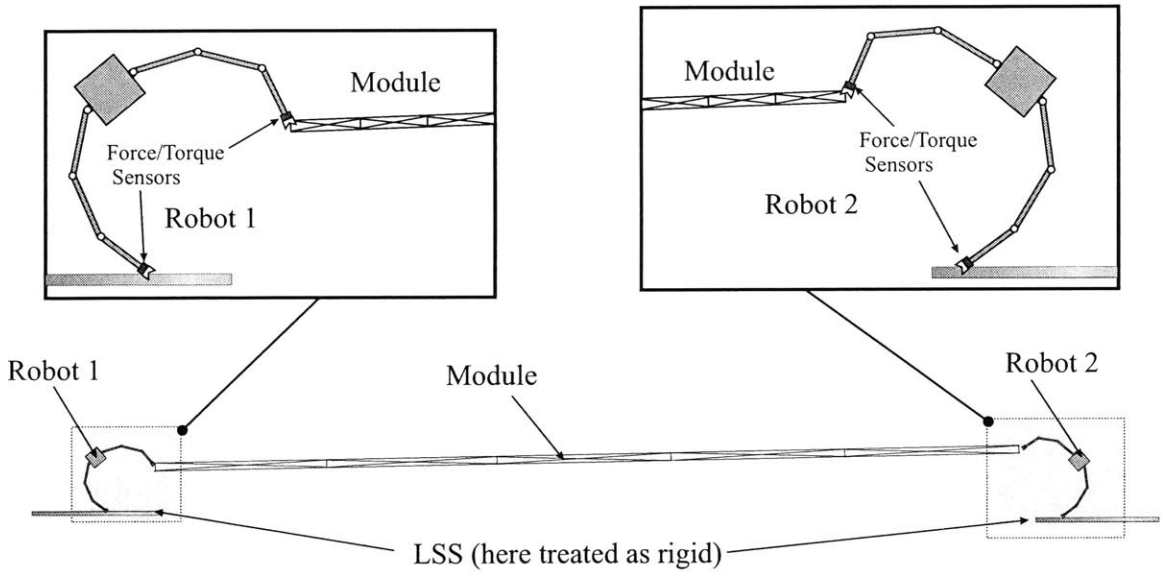

Figure 2.1. Manipulation of a large flexible structural module by a team of robots mounted on the LSS. Here, the LSS is assumed to be rigid.

The manipulation of such a large flexible structure in the close proximity of the LSS is a challenging task. Fig. 2.2 and 2.3 show simulation results for the manipulation of a 200m beam by two 20m robots. The robots grasp the beam at its ends and move it by 6m in the Y direction (normal to the beam neutral axis) within 30 sec. The robots are

controlled by joint PD controllers. The design of the joint PD controllers ignores the flexibility of the beam. Fig. 2.2 shows that robots apply to the module excessive oscillatory forces. For example the forces that robots apply in the X axis do not result in moving the beam. Instead, they induce tensile and compressive stresses that can damage the beam.

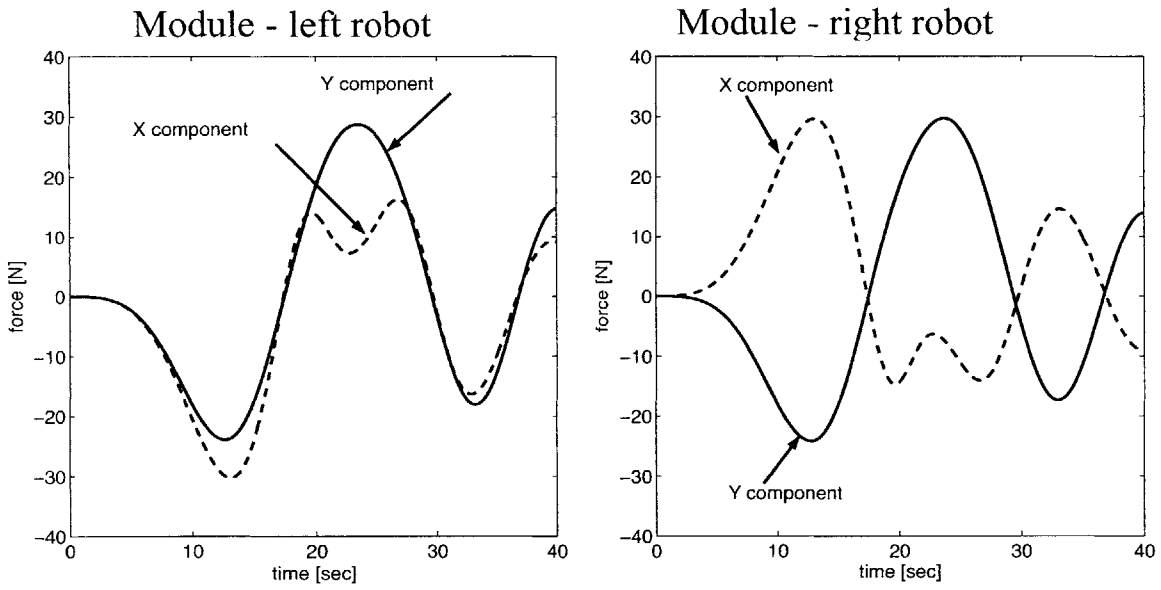

Figure 2.2. Interaction forces between the module and two robots that maneuver it. The robots are controlled by joint PD controllers.

Fig. 2.3 shows that the interaction of the large flexible structure with the robots, which are controlled by joint PD controllers, results in large structural deflection and residual vibration in the module that damps slowly. The positioning accuracy is poor because the position of the beam CM oscillates around the desired final value (zero). The resulting distance between the beam ends and the corresponding mating points in the LSS is large and prevents the operation of the latching mechanisms that connect the LSS with the module. Therefore, the performance shown in Fig. 2.2 and 2.3 is not satisfactory. It is desirable to plan and control the robots so that they manipulate the module into its pre-

assembly position accurately while exciting low residual vibration in the module. This is achieved by the planning and control architecture described in Sections 2.4 to 2.7.

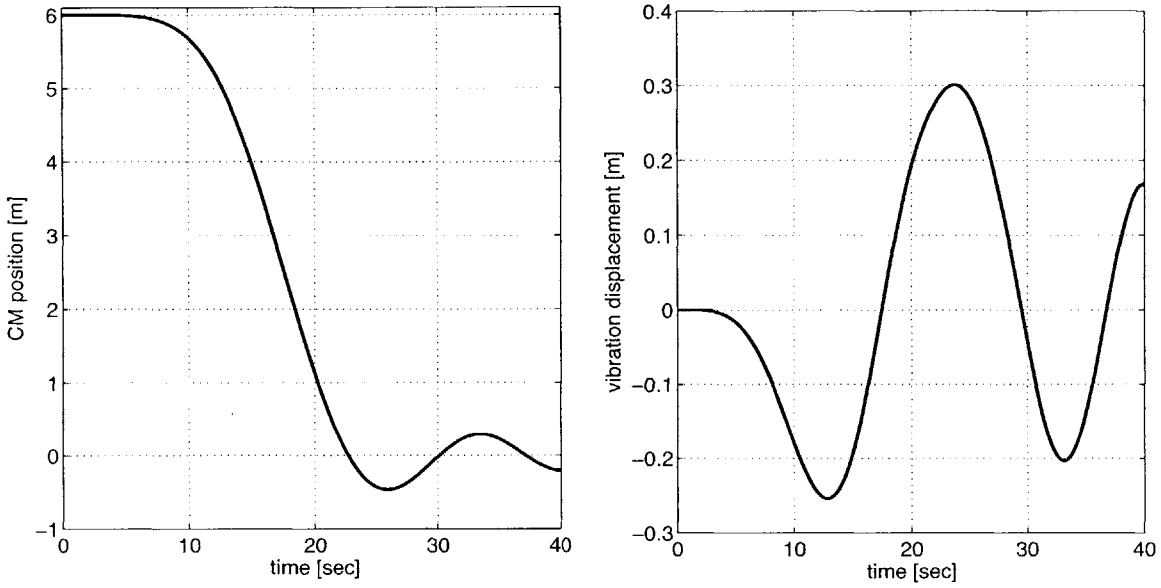

Figure 2.3. Left: Beam CM position response. Right: Vibration displacement in the left beam end. The beam is maneuvered by two robots that are controlled by joint PD controllers.

2.3 System Modeling

A planar model of a representative system considered in this study is shown in Fig. 2.4. Two redundant planar robots manipulate a long flexible beam (module) from its initial position in the proximity of the LSS to its pre-assembly position. While the examples considered in this thesis are planar, the approach can be extended to the general three-dimensional case.

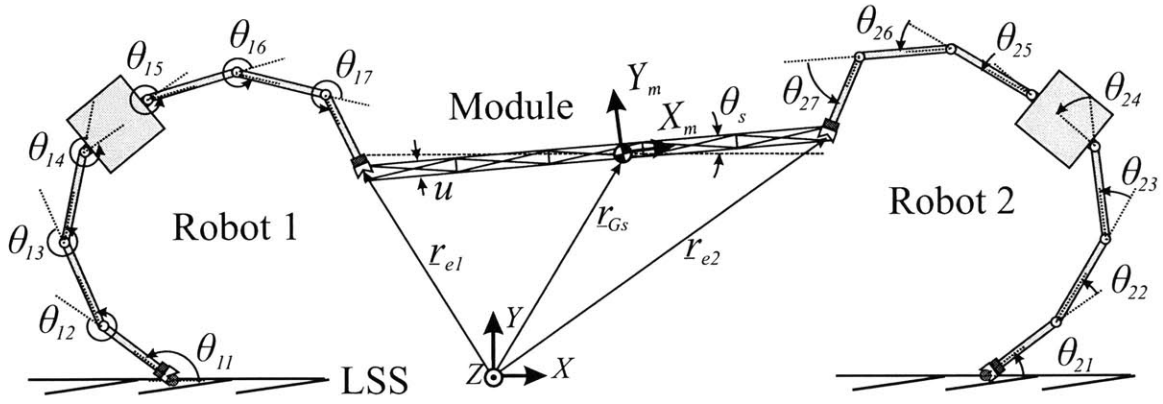

Figure 2.4. Planar model for the manipulation of a large flexible structure by two robots mounted on a rigid base structure.

2.3.1 Robot Model

Each robot is assumed to have N rigid links, where N>2 so that it is redundant with respect to positioning its end-effector at inertial position $\underline{r}_{ei}$. Each robot firmly grasps the module and the connection acts as a pinned joint. This means that each robot can apply forces to the module but no moments. The configuration of each robot is described by its joint angle vector $\underline{\theta}_i$, where i=1 refers to the left robot and i=2 to the right robot. θ_{ij} denotes the j-th link of robot i. The dynamics of each robot in joint space are [29]:

$$\underline{B}_i(\underline{\theta}_i)\ddot{\underline{\theta}}_i + \underline{\eta}_i(\underline{\theta}_i, \dot{\underline{\theta}}_i) = \underline{\tau}_i - \underline{J}_{ei}^T(\underline{\theta}_i)\underline{f}_{si} \quad , \ i = 1, 2 \tag{2.1}$$

where $\underline{B}_i(\underline{\theta}_i)$ is the robot mass matrix, $\underline{\eta}_i(\underline{\theta}_i, \dot{\underline{\theta}}_i)$ contains nonlinear and friction terms, $\underline{\tau}_i$ is the N×1 vector of joint torques, $\underline{f}_{si}$ is the 2×1 force vector applied by robot i to the module and $\underline{J}_{ei}(\underline{\theta}_i)$ is the Jacobian matrix for the robot end-efector position $\underline{r}_{ei}$ [29]:

$$\dot{\underline{r}}_{ei} = \underline{J}_{ei}(\underline{\theta}_i)\dot{\underline{\theta}}_i \tag{2.2}$$

All force and position vectors are expressed in the inertial frame XYZ. The study of the robot-module dynamic interaction is based on the robot dynamics expressed in its operation space, which here coincides with the inertial frame XYZ [19]:

$$\underline{B}_{Ai}(\underline{\theta}_i)\ddot{\underline{r}}_{ei} + \underline{\eta}_{Ai}(\underline{\theta}_i, \dot{\underline{\theta}}_i) + \underline{D}_{Ai}(\underline{\theta}_i)\dot{\underline{r}}_{ei} = \underline{\gamma}_i - \underline{f}_{si} \tag{2.3}$$

where $\underline{\eta}_{Ai}(\underline{\theta}_i, \dot{\underline{\theta}}_i)$ are nonlinear terms and $\underline{D}_{Ai}(\underline{\theta}_i)$, $\underline{B}_{Ai}(\underline{\theta}_i)$ are the 2×2 damping and inertia matrices of the robot with respect to its operation space:

$$\underline{B}_{Ai}(\underline{\theta}_i) = (\underline{J}_{ei}\underline{B}_i^{-1}\underline{J}_{ei}^T)^{-1} \tag{2.4}$$

The vector $\underline{\gamma}_i$ is the contribution of the end-effector forces due to joint actuation $\underline{\tau}_i$. The robot joint torques $\underline{\tau}_i$ that are equivalent to $\underline{\gamma}_i$ are:

$$\underline{\tau}_i = \underline{J}_{ei}^T \underline{\gamma}_i \tag{2.5}$$

2.3.2 Module Model

For the planar system considered here, the module is modeled as a long slender Euler-Bernoulli beam. A sample beam-like structure is shown in Fig. 2.5. The two robots grasp the beam at its ends (grasping points).

A coordinate system $X_m Y_m Z_m$ is attached to the beam at its center of mass so that the axis X_m coincides with the beam neutral axis, Fig. 2.4. The rigid body motion of the beam is described by its orientation θ_s and the inertial position $\underline{r}_{Gs}$ of its centre of mass. Given the nature of the task considered here, θ_s and $\dot{\theta}_s$ are assumed to be relatively small. The beam deflection u in the Y_m axis is approximated by Q assumed modes [24]:

$$u(x_m, t) = \sum_{i=1}^{Q} \{q_{si}(t)\phi_i(x_m)\} = \underline{q}_s^T \underline{\phi}(x_m) \tag{2.6}$$

$$\underline{q}_s = \begin{bmatrix} q_{s1} & \cdots & q_{sQ} \end{bmatrix}^T \quad , \quad \underline{\phi}(x_m) = \begin{bmatrix} \phi_1(x_m) & \cdots & \phi_Q(x_m) \end{bmatrix}^T \tag{2.7}$$

where q_{si} is the i-th modal coefficient. Here ϕ_i is taken to be the i-th mode shape of the free-free beam. The vector $\underline{x}_s$ contains the beam's generalized coordinates [24]:

$$\underline{x}_s = \begin{bmatrix} \underline{r}_{Gs}^T & \theta_s & \underline{q}_s^T \end{bmatrix}^T \tag{2.8}$$

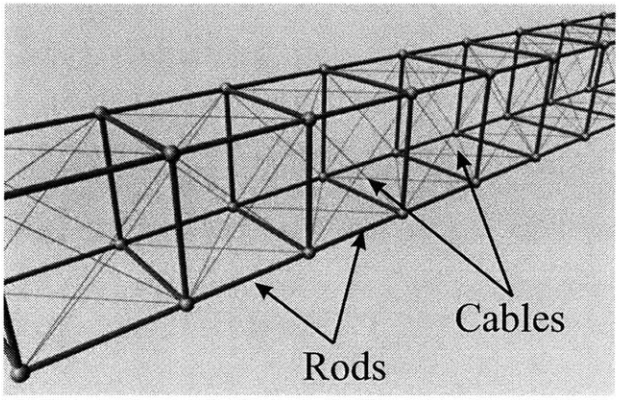

Figure 2.5. Sample beam-like LSS module made of rods and cable elements.

The module dynamics are derived by expressing the position of each beam element as a function of $\underline{x}_s$ and applying the Langrangian principle [24]. The assumption of small θ_s and $\dot{\theta}_s$ simplifies the derivations. The resulting beam dynamics are:

$$\underline{M}_{sr} \ddot{\underline{x}}_{sr} = \underline{W}_{sr} \begin{bmatrix} \underline{f}_{s1}^T & \underline{f}_{s2}^T \end{bmatrix}^T \tag{2.9}$$

$$\ddot{\underline{q}}_s + 2\underline{Z}_s \underline{\Omega}_s \dot{\underline{q}}_s + \underline{\Omega}_s^2 \underline{q}_s = \underline{W}_{sv} \begin{bmatrix} \underline{f}_{s1}^T & \underline{f}_{s2}^T \end{bmatrix}^T = \begin{bmatrix} h_1(t) & \cdots & h_Q(t) \end{bmatrix}^T \tag{2.10}$$

where $\underline{x}_{sr} = \begin{bmatrix} \underline{r}_{Gs}^T & \theta_s \end{bmatrix}^T$ contains the beam rigid body coordinates, $\underline{f}_{si}$ is the force applied by robot i to the beam, $\underline{M}_{sr}$ is the beam mass matrix for the beam rigid body motion, $\underline{Z}_s$ and $\underline{\Omega}_s$ are the beam modal damping and natural frequency matrices, and $\underline{W}_{sr}$, $\underline{W}_{sv}$ are grasp matrices [26]. The function $h_i(t)$ is the excitation of the assumed mode i caused by

the forces $\underline{f}_{si}$ that robots apply to the beam. In this study, it is assumed that the effects of orbital mechanics are negligible, the kinematic and dynamic parameters of the module (inertial properties, vibration model) are relatively well known and that initially the beam is at rest ($\underline{q}_s(0) = \dot{\underline{q}}_s(0) = \underline{0}$).

2.4 Planning and Control Architecture Overview

The system of interest (robots and module) is a complex nonlinear system. The inputs of this system are the robot joint torques $\underline{\tau}_i$. The outputs of interest are the beam motion and vibration response, and the motion of the robot joint angles $\underline{\theta}_i$. The planning and control of such a complex nonlinear system so that the task objectives are achieved optimally (accurate positioning and low residual vibration in the module) is difficult and complicated [7, 8, 11, 26].

The key idea of the planning and control architecture is to divide the system into interacting mechanical subsystems instead of treating the system as a whole. These subsystems are the robots and the module. The subsystems interact through the forces $\underline{f}_{si}$ that robots apply to the module. Since the dynamics of the module can be described well by simple dynamic models (Section 2.3), it is relative easy to plan the desired interaction forces $\underline{f}_{sid}$ such that the beam is positioned accurately and with low residual vibration. Robots control the forces $\underline{f}_{si}$ that they apply to the module so that $\underline{f}_{si}$ track the desired interactive forces $\underline{f}_{sid}$. At the same time robots exploit their redundancy to avoid undesirable configurations.

Fig. 2.6 shows the planning and control architecture (Architecture for Minimum Vibration Manipulation - AMVM) for the cooperative manipulation of a large flexible module by a team of robots mounted on a rigid base structure. The architecture consists of two parts. Robots plan and control cooperatively the forces $\underline{f}_{si}$ they apply to the module (endpoint forces). At the same time, each robot individually plans and controls the motion of its redundant joints $\underline{\theta}_i$. The total torque actuation for each robot $\underline{\tau}_i$ is the sum of the actuation output of the end-effector force controller $\underline{\tau}_{Ei}$ and the actuation output of the robot motion controller $\underline{\tau}_{Mi}$.

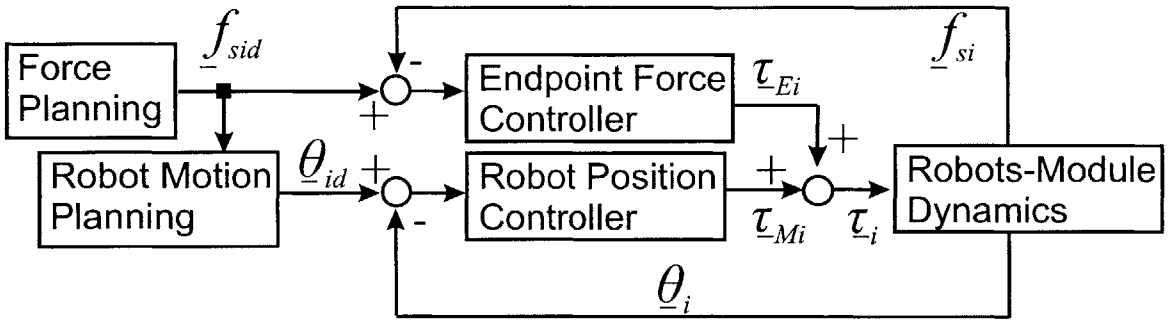

Figure 2.6. Overview of the Architecture for Minimum Vibration Manipulation (AMVM).

The force planning algorithm calculates the desired forces $\underline{f}_{sid}$ that each robot needs to apply to the module so that the module is positioned accurately and with low levels of residual vibration. Robots control the forces $\underline{f}_{si}$ to track the desired ones $\underline{f}_{sid}$ by using the endpoint force controller.

The endpoint force controller does not directly control the motion of the robot joints. Each robot should avoid certain joint configurations that can damage it or limit its performance. This problem is addressed by the second part of AMVM , the robot motion planning and control algorithms. Since each robot already controls the two force

components of $\underline{f}_{si}$ (planar case), it can control at most N-2 joint angles (its redundant degrees of freedom). In this study each robot controls its first N-2 joints (θ_{i1} to $\theta_{i,N-2}$). The endpoint force controller output $\underline{\tau}_{Ei}$ is nonzero for all robot joints whereas the position controller output $\underline{\tau}_{Mi}$ is nonzero for the first N-2 joints.

The control actions of the AMVM architecture for each robot is shown in Fig. 2.7. Each robot controls the force at its end-effector (X_e, Y_e axes) and the position of the origin of the X_a, Y_a frame (or equivalently the first N-2 joint angles).

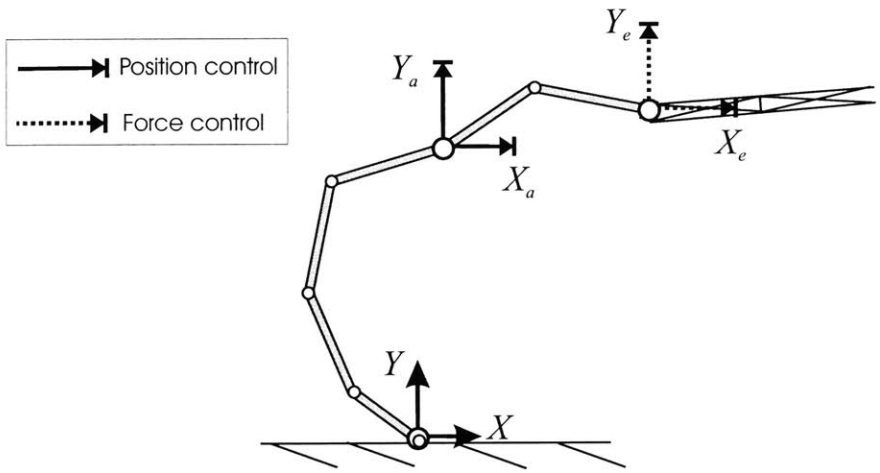

Figure 2.7. Control actions for each robot in AMVM.

The design of the robot controllers is based on the assumed set of specifications shown in Table 2.1. The duration of the manipulation task is Δt. $\delta \underline{r}_{Gs}$ is the maximum allowable positioning error for the beam CM $\underline{r}_{Gs}$. $\delta\theta_s$ is the maximum allowable positioning error for the beam orientation θ_s. δu_{tip} is the maximum allowable residual vibration at the beam ends.

Beam position error $\delta \underline{r}_{Gs}$	[m]	± 0.10
Beam orientation error $\delta\theta_s$	[deg]	± 0.05
Residual vibration in beam ends δu_{tip}	[m]	± 0.03

Table 2.1. Specifications for the design of the AMVM planning and control architecture.

2.5 Force Planning

This section describes a simple algorithm for the planning of the desired forces $\underline{f}_{sid}$ that robots are to apply to the module. It is assumed that initially the beam is located at $\underline{r}_{Gs}(0) = [\underline{0} \quad 0]^T$, $\theta_s(0) = 0$, and that the desired module position is $\underline{r}_{Gs}(\Delta t)$, $\theta_s(\Delta t)$. The objective is to plan the desired forces $\underline{f}_{sid}$ so that when they are applied by the robots to the module, the beam is transported to its desired position, within time duration Δt and with low levels of residual vibration. For the planar case considered here, each force $\underline{f}_{sid}$ is expressed in its components parallel to the inertial axis X and Y:

$$\underline{f}_{sid} = [f_{siXd} \quad f_{siYd}]^T \quad , \quad \mathrm{i} = 1, 2 \tag{2.11}$$

It is desirable to provide smooth force commands so that they can be tracked easily by the endpoint force controller. For this reason, each force component $\underline{f}_{sijd}(t)$ is expressed as a sum of M sinusoids:

$$f_{sijd}(t) = \sum_{k=1}^{M} \{a_{ijk} \sin(\omega_{pi} t)\} \quad , \quad \mathrm{i} = 1, 2 \quad , \quad \mathrm{j} = X \, , \, Y \tag{2.12}$$

The frequencies ω_{pi} are chosen to lie within the bandwidth of the endpoint force controller, which will be discussed in Section 2.6. The parameters a_{ijk} are calculated by imposing three constraints:

1. The force commands f_{sijd} are smooth. Since f_{sijd} are a sum of smooth functions, the smoothness condition has to be imposed only at t=0 and t= Δt :

$$f_{sijd}(\Delta t) = \sum_{k=1}^{M} \{a_{ijk} \sin(\omega_{pi} \Delta t)\} = 0 \tag{2.13}$$

$$\dot{f}_{sijd}(0) = \sum_{k=1}^{M} \{a_{ijk} \omega_{pi}\} = 0 \tag{2.14}$$

$$\dot{f}_{sijd}(\Delta t) = \sum_{k=1}^{M} \{a_{ijk} \omega_{pi} \cos(\omega_{pi} \Delta t)\} = 0 \tag{2.15}$$

2. The force inputs $\underline{f}_{sid}$ cause the beam to translate by $\underline{r}_{Gs}(\Delta t)$ and rotate by $\theta_s(\Delta t)$, so that it is transported into its desired position:

$$\int_0^{\Delta t} \int_0^{\Delta t} \underline{W}_{sr} \begin{bmatrix} \underline{f}_{s1} \\ \underline{f}_{s2} \end{bmatrix} dt dt = \underline{M}_{sr} \begin{bmatrix} \underline{r}_{Gs}(\Delta t) \\ \theta_s(\Delta t) \end{bmatrix} \tag{2.16}$$

where the matrices $\underline{W}_{sr}$, $\underline{M}_{sr}$ are defined in Section 2.3.

3. The force inputs $\underline{f}_{sid}$ induce low levels of residual vibration in the beam ends (grasping points). This is achieved by inducing zero residual vibration in the modes that participate more in the response of the beam ends. Residual vibration in mode i is eliminated if its excitation h_i (Eq. 2.10) satisfies the condition [6]:

$$\left\| \int_0^{\Delta t} h_i(t) e^{-s_i t} dt \right\| = 0 \tag{2.17}$$

where $s_i = -\zeta_i \omega_{ni} + j\omega_{ni}\sqrt{1-\zeta_i^2}$ is the pole of beam mode i, and ζ_i, ω_i are the damping ratio and natural frequency of beam mode i. This condition imposes two equations, because the real and imaginary parts of Eq. 2.17 must equal zero.

The vibration parameters of the system probably are not known exactly. Therefore, the result of Eq. 2.17 should be robust to variations of the beam pole locations s_i. The condition for robust minimization of residual vibration in mode i is obtained by differentiating Eq. 2.17 with respect to s_i:

$$\left\| \int_0^{\Delta t} th_i(t) e^{-s_i t} dt \right\| = 0 \tag{2.18}$$

Residual vibration in the beam ends is minimized if Eq. 2.17 and 2.18 are imposed to all dominant modes of the beam. The selection of these modes is based on observability properties of the system, for example by choosing the modes that have the largest Hankel singular values hsv_i [12]:

$$hsv_i = \left\| \underline{W}_{svi} \right\|_2^2 \Big/ 4\zeta_i \omega_i \tag{2.19}$$

$\underline{W}_{svi}$ is the i-th row of the grasp matrix $\underline{W}_{sv}$ (see Eq. 2.10 in Section 2.3), and $\|\cdot\|_2$ denotes the 2-norm of a vector.

The constraints imposed by Eq. 2.13 to 2.19 create a system of equations with unknowns a_{ijk}. Assuming small θ_s, these equations are simplified into a linear system:

$$\underline{A}_p \underline{a} = \underline{b}_p \tag{2.20}$$

where the vector $\underline{a}$ contains the unknown parameters a_{ijk} and $\underline{A}_p$, $\underline{b}_p$ are constant matrices. If M is large enough, then the number of unknowns a_{ijk} is larger than the number of equations and the system has infinite solutions. The chosen solution is:

$$\underline{a} = \underline{A}_p^{+} \underline{b}_p \tag{2.21}$$

where $\underline{A}_p^+$ is the pseudo-inverse of $\underline{A}_p$ [26]. This solution minimizes the norm $\|\underline{a}\|_2^2 = \sum_i \sum_j \sum_k a_{ijk}^2$. The resulting force profiles are suboptimal with respect to minimizing the metric $I = \int_0^{\Delta t} \sum_i \|\underline{f}_{si}\|_2^2 dt$ (the magnitude of the forces applied by the robots to the module). However, this algorithm is computationally efficient, provides smooth force profiles and distributes loads evenly among robots.

Residual vibration elimination can also be achieved by applying the input shaping method [32, 34]. In this method, a proper filter modifies an initial force command profile such that its output satisfies Eq. 2.17 and therefore results in minimum residual vibration. This filtering induces a time delay, which equals at least half the period of the module lowest mode. The method described here is somewhat more general than input shaping as it can be modified easily to deal with nonzero initial vibration conditions.

Assuming that robots control the forces $\underline{f}_{si}$ that they apply to the module so that they track perfectly the commands $\underline{f}_{sid}$. If the dynamic properties of the module are known exactly, then the forces $\underline{f}_{sid}$ will cause the beam to be positioned accurately and with low residual vibration. If the vibration parameters of the beam are known within some reasonable error ($\pm 10\%$), the beam will be positioned accurately and with small residual vibration (due to Eq. 2.18). If the inertial parameters of the beam are not known exactly (or if they have been modified, for example due to thermal warping [22]), then the forces $\underline{f}_{sid}$ will not cause the beam to be positioned accurately. These positioning errors can be reduced by either adding an impedance control action [15], or by updating

the desired force profiles $\underline{f}_{sid}$ by a guidance loop. In the late case, the force planning algorithm provides updated force profiles $\underline{f}_{sid}$ using estimates of the current state of the beam that are calculated from measurements of the robot state $\underline{\theta}_i$, $\underline{\dot{\theta}}_i$. Any force tracking errors $\underline{\tilde{f}}_{si} = \underline{f}_{sid} - \underline{f}_{si}$ result in increased positioning error and residual vibration in the module.

2.6 Endpoint Force Controller Design

2.6.1 Force Controller Overview

The objective of the robot endpoint force controller is to have the forces $\underline{f}_{si}$ that robots apply to the module (endpoint forces) track the desired forces $\underline{f}_{sid}$. The actuator output of the controller for each robot $\underline{\tau}_{Ei}$ is the sum of an action from a centralized controller ${}^{C}\underline{\tau}_{Ei}$, an action from each robot's decentralized controller ${}^{D}\underline{\tau}_{Ei}$, and a feed-forward term ${}^{F}\underline{\tau}_{Ei}$, Fig. 2.8:

$$\underline{\tau}_{Ei} = {}^{C}\underline{\tau}_{Ei} + {}^{D}\underline{\tau}_{Ei} + {}^{F}\underline{\tau}_{Ei} \tag{2.22}$$

The centralized control action is a state feedback controller that modifies the system dynamics so that the forces $\underline{f}_{si}$ can be controlled more easily. It provides joint torque actuation ${}^{C}\underline{\tau}_{Ei}$ for all robots. This controller exploits robot cooperation to enhance the performance of the endpoint force controller.

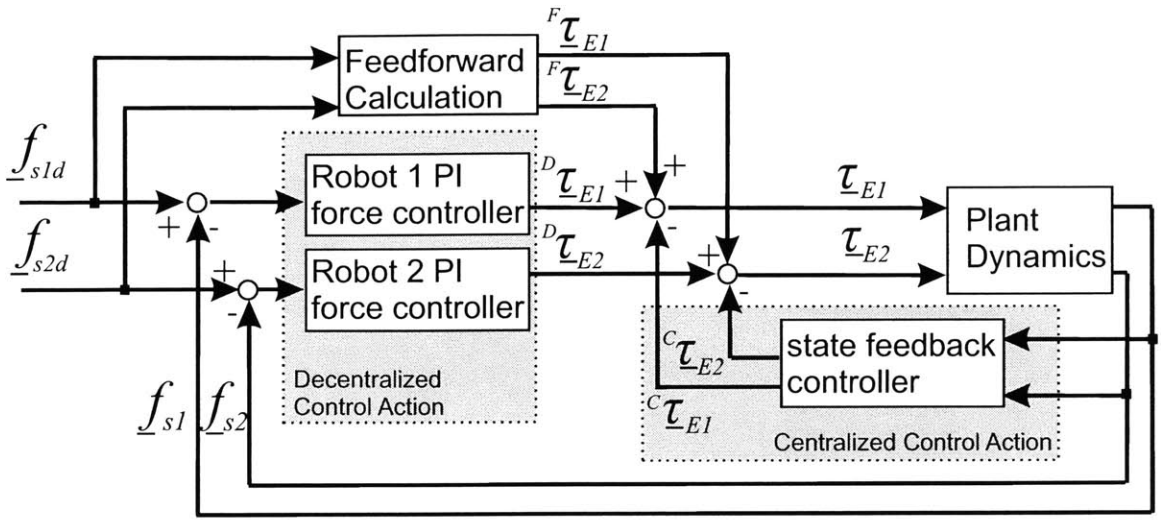

Figure 2.8. Endpoint force control architecture.

Each robot has its own decentralized PI controller for every component of $\underline{f}_{si}$. The input to each PI controller is the tracking error $\underline{\tilde{f}}_{si}$ and the output is a joint torque action ${}^{D}\underline{\tau}_{Ei}$ for this specific robot. The decentralized controllers provide direct closed loop action that affects the closed loop bandwidth and steady state errors.

2.6.2 Robots – Module Dynamic Model

Combining the dynamics of the module and the robots and linearizing the system around a representative robot configuration (so that the robot matrices $\underline{B}_{Ai}$ and $\underline{D}_{Ai}$ are constant), the plant dynamics are described by a linear MIMO system (the analytic derivation of the linearized system dynamics is shown in appendix A):

$$\begin{aligned} \dot{\underline{x}}_F &= \underline{A}_F \underline{x}_F + \underline{B}_F \underline{\gamma} \\ \underline{f}_s &= \underline{C}_F \underline{x}_F \end{aligned} \qquad (2.23)$$

$$\underline{\gamma} = \begin{bmatrix} \underline{\gamma}_1^T & \underline{\gamma}_2^T \end{bmatrix}^T$$

$$\underline{f}_s = \begin{bmatrix} \underline{f}_{s1}^T & \underline{f}_{s2}^T \end{bmatrix}$$

where $\underline{x}_F$ is the state of the robots-module system, and $\underline{\gamma}_i$ is the contribution of the end-effector forces due to joint actuation $\underline{\tau}_i$ (Eq. 2.5). The plant can be equivalently described by a transfer matrix $\underline{G}_F(s)$. It can be shown that the plant zeros are the poles of the free-free beam, and that the plant poles are the poles of the free-free beam and the poles of the free-free beam augmented by proper mass and damper elements that correspond to $\underline{B}_{Ai}$ and $\underline{D}_{Ai}$. Since space structures have poor modal damping [12], the poles and zeros of the plant are located very close to the imaginary axis.

2.6.3 Endpoint Force Controller Design

Force controllers usually contain proportional (P) and integral (I) terms, and do not contain derivative (D) terms to avoid the differentiation of noisy force signals [29]. A simple control architecture for the endpoint force controller is to have each robot to control its own endpoint force $\underline{f}_{si}$ without considering the control performance in the other robots of the team. A proper PI controller for each force component would be (the double pole at $s = 0$ compensates the zeros of the plant at $s = 0$):

$$G_{FCj}(s) = \frac{K_{Pj}s + K_{Ij}}{s^2} \quad , \quad j = X, Y \tag{2.24}$$

The beam is considered rigid in the X_m direction and flexible in the Y_m direction. Since the beam orientation θ_s is small, the axes X_m Y_m almost coincide with the axes X Y. Therefore robots use different PI controllers G_{CFX}, G_{CFY} to control the X and Y

components of $\underline{f}_{si}$ without considering the beam orientation θ_s. The output of the decentralized PI controller for each robot is:

$$^{D}\underline{\gamma}_{Ei} = \begin{bmatrix} G_{FCX}(s) & \\ & G_{FCY}(s) \end{bmatrix} \{\underline{\tilde{f}}_{si}\} \tag{2.25}$$

$$^{D}\underline{\tau}_{Ei} = \underline{J}_{ei}^{T}\, ^{D}\underline{\gamma}_{Ei} \tag{2.26}$$

where $\underline{\tilde{f}}_{si} = \underline{f}_{sid} - \underline{f}_{si}$ is the tracking error of $\underline{f}_{si}$.

This control architecture results in slow closed loop bandwidth and oscillatory response. The reason is that the poles and zeros of $\underline{G}_F(s)$ are located near the imaginary axis and small gains in the PI controllers can make the closed loop system unstable. Therefore, if robots use only decentralized PI controllers, the closed loop system will be too slow to track the commands $\underline{f}_{sid}$ that can maneuver the beam within duration Δt.

This problem is overcome by combining the simple decentralized PI controllers with a centralized force control action, as shown in Fig. 2.8. The centralized force controller modifies the system dynamics. The decentralized PI controllers of each robot, Eq. 2.25 to Eq. 2.26, now control the modified plant. The centralized force controller is a state feedback control law:

$$\begin{bmatrix} ^{C}\underline{\gamma}_{E1} \\ ^{C}\underline{\gamma}_{E2} \end{bmatrix} = -\underline{K}_F \underline{x}_F \tag{2.27}$$

$$^{C}\underline{\tau}_{Ei} = \underline{J}_{ei}^{T}\, ^{C}\underline{\gamma}_{Ei} \tag{2.28}$$

The state $\underline{x}_F$ is estimated from measurements of $\underline{f}_{si}$ through a linear observer [1]. The state feedback gain $\underline{K}_F$ depends on the selection of the desired poles of the dynamics of

the modified plant. The state matrix of the modified plant is $\underline{A}_F^* = \underline{A}_F - \underline{B}_F \underline{K}_F$. The i-th pole of $\underline{A}_F^*$ is chosen to be better damped and somehow faster than the i-th pole of $\underline{A}_F$. The desired poles of $\underline{A}_F^*$ are located on the left of its zeros. This pole-zero placement allows the application of larger gains K_{Pj} and K_{Ij} in the decentralized PI controllers without making the closed loop system unstable.

A feed-forward component is added. It is a model-based action which uses the inverse dynamics of the nominal plant dynamics $\underline{G}_F^{-1}(s)$, see Appendix A:

$$\begin{bmatrix} {}^F\underline{\Gamma}_{E1}(s) \\ {}^F\underline{\Gamma}_{E2}(s) \end{bmatrix} = \underline{G}_F^{-1}(s) \begin{bmatrix} \underline{F}_{s1d}(s) \\ \underline{F}_{s2d}(s) \end{bmatrix} \tag{2.29}$$

$${}^F\underline{\tau}_{Ei} = \underline{J}_{ei}^T {}^F\underline{\gamma}_{Ei} \tag{2.30}$$

where ${}^F\underline{\Gamma}_{Ei}(s)$, $\underline{F}_{sid}(s)$ are the Laplace transformations of the actuation ${}^F\underline{\gamma}_{Ei}$ and the desired endpoint forces $\underline{f}_{sid}$.

2.6.4 Controller Robustness

The design of the control gains $\underline{K}_F$, K_{Pj} and K_{Ij} is based on a nominal linear plant (Eq. 2.23) that has been derived using a constant mass matrix $\underline{B}_{Ai}$ for each robot. In reality, the inertia $\underline{B}_{Ai}$ of each robot depends on its configuration. As the robot moves and its inertia varies, the plant dynamics change. It is desirable to minimize the effect of this change in the performance of the robot endpoint force controller.

As the beam "feels" more robot mass, the distance between the poles and zeros of $\underline{G}_F(s)$ increase and smaller gains K_{Pj} and K_{Ij} can cause the closed loop system to

become unstable. Therefore, the controller design becomes more robust to robot configuration if the beam "feels" that robots have small inertia, regardless of their configuration.

The beam "feels" that each robot has inertia $\underline{B}_{Ai}$, which can be expressed as:

$$\underline{B}_{Ai} = \underline{U}(\underline{\theta}_i)\begin{bmatrix}\mu_{\max}(\underline{\theta}_i) & \\ & \mu_{\min}(\underline{\theta}_i)\end{bmatrix}\underline{U}(\underline{\theta}_i)^T \tag{2.31}$$

where the columns of $\underline{U}$ are the robot's principal axis of inertia (in operation space) and $\mu_{\max}$, $\mu_{\min}$ are the eigenvalues of $\underline{B}_{Ai}$. The beam "feels" that a robot has small inertia, regardless of its configuration if $\mu_{\max}$, $\mu_{\max} - \mu_{\min}$ are small compared to the beam inertia.

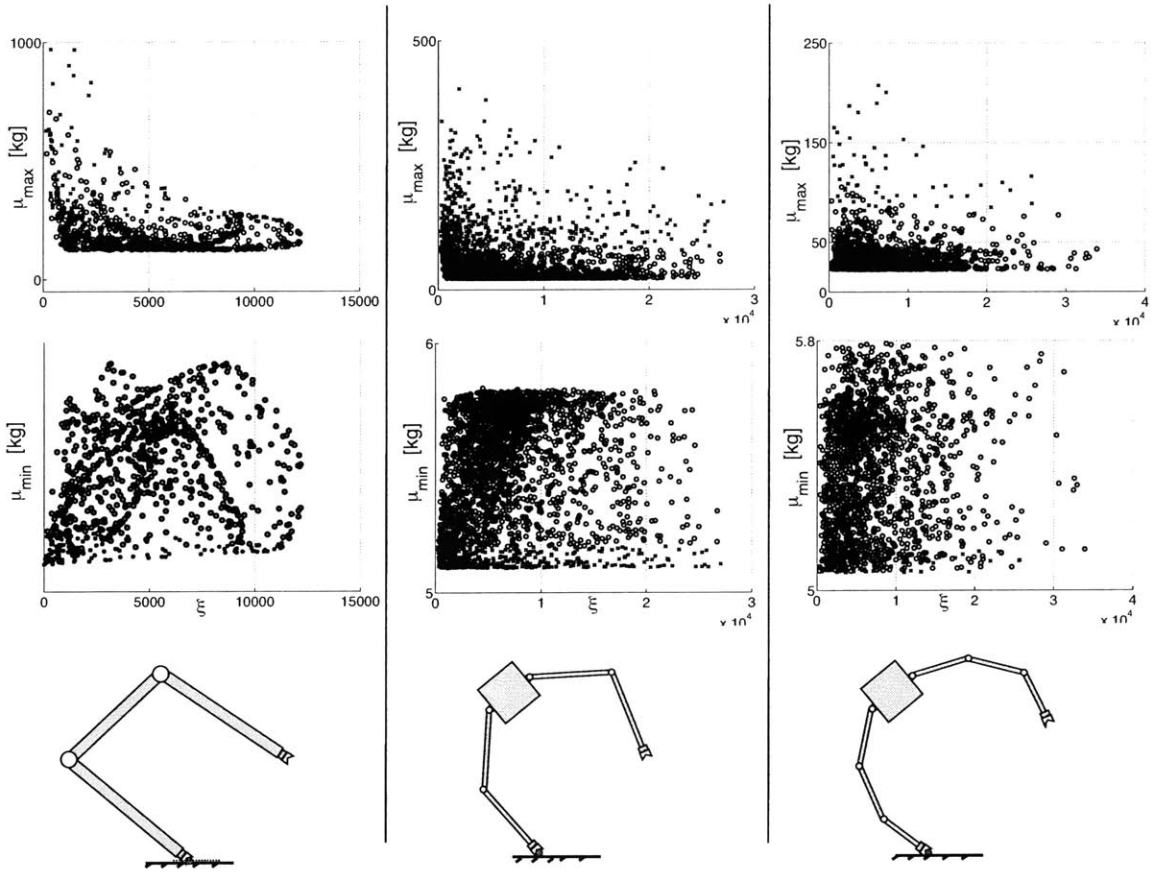

Figure 2.9. Inertial properties of three robot designs with respect to their operation space.

The parameters μ_{max}, μ_{min} depend on the robot size and mass and also on the mechanical design of the robot. Fig. 2.9 shows the inertial properties μ_{max}, μ_{min} of three robot designs that have the same total length (20 m) and total mass (350 kg). The properties μ_{max}, μ_{min} are calculated for a large number of arbitrary configurations and plotted against the corresponding value of the manipulability metric ξ [47]. The first design is a simple three-link robot with evenly distributed weight. The other two designs are a five-link and a seven-link robot with the majority of their weight concentrated on their middle link (which acts as the robot body).

Fig. 2.9 shows that the three-link design is not appropriate to apply the endpoint force controller as its inertia is large (μ_{max} >110 kg). The five-link and seven-link designs have lower inertia (μ_{max} <50 kg). All designs have large μ_{max} near singular configurations (very low ξ). The parameters μ_{max}, μ_{min} are plotted against the manipulability metric ξ to show that the beam can "feel" that a robot is heavy at certain robot configurations (noted with 'x' in Fig. 2.9) that are away from the robot's singular configurations. These undesirable configurations for the five-link robot occur when the last joint angle approaches zero ($\theta_{15} \rightarrow 0$). The avoidance of such configurations limits severely the robot's workspace. The undesirable configurations for the seven-link robot occur when the last two joint angles approach zero ($\theta_{16} \rightarrow 0$ and $\theta_{17} \rightarrow 0$). The avoidance of these configurations is achieved by proper joint planning and control without imposing severe limits to the robot motion.

The second way to improve the robustness of the force controller is to implement an active damping action:

$$\underline{\tau}_{damp} = -\underline{J}_{ei}^{T}\underline{D}_{Aid}\dot{\underline{r}}_{ei} = -\underline{J}_{ei}^{T}\underline{D}_{Aid}\underline{J}_{ei}\dot{\underline{\theta}}_{i} \tag{2.32}$$

This term provides damping that is constant with respect to the robot operational space and does not depend on the robot configuration. This can be thought as adding dashpots of constant damping rate $\underline{D}_{Aid}$ on the ends of the beam. Simulation results show that this damping action reduces the dependence of the closed loop poles on the robot configuration.

2.7 Robot Motion Planning and Control

The second part of AMVM is the robot motion planning and control algorithm, Fig. 2.6. This part provides direct control over the redundant joints of the robot and makes the robot able to avoid undesirable configurations and obstacles.

2.7.1 Robot Motion Planning

Fig. 2.10 shows the robot motion planning and control algorithm of the AMVM. The desired joint angles $\underline{\theta}_{id}$ for each robot are calculated by a priority-based inverse kinematics algorithm [26]. The first priority is that the desired robot motion must be compatible with a prediction of the motion $\hat{\underline{r}}_{ei}(t)$ of the corresponding beam end when the forces applied by the robots to the module $\underline{f}_{si}$ equal the desired ones $\underline{f}_{sid}$:

$$\underline{J}_{ei}(\underline{\theta}_{id})\dot{\underline{\theta}}_{id} = \dot{\hat{\underline{r}}}_{ei} \tag{2.33}$$

This prediction $\hat{\underline{r}}_{ei}(t)$ is calculated from a simple dynamic model of the beam.

Since only the first N-2 joints of the robot are controlled, the robot motion $\underline{\theta}_{id}$ will be compatible with the beam motion if the distance between the origin of the frame $X_a Y_a Z_a$ shown in Fig. 2.7 and the estimated motion $\hat{\underline{r}}_{ei}(t)$ is less than the sum of the lengths of the last two robot links. Since the calculated $\hat{\underline{r}}_{ei}(t)$ can deviate from the real value $\underline{r}_{ei}(t)$, robot motion planning should avoid to plan the last two robot joints to take values near zero.

The second priority of the inverse kinematics algorithm exploits robot redundancy so that the robot avoids undesirable configurations, joint limits and obstacles. This is achieved by planning $\underline{\theta}_{id}$ to minimize a smooth potential function $W(\underline{\theta}_i)$ [18]. The resulting desired motion for the robot joints is:

$$\dot{\underline{\theta}}_{id} = \underline{J}_{ei}^{+} \dot{\hat{\underline{r}}}_{ei} - \underline{J}_{ei}^{\#} \left(\frac{\partial W}{\partial \underline{\theta}_i} \bigg|_{\underline{\theta}_{id}} \right)^T \tag{2.34}$$

where $\underline{J}_{ei}^{+}$ is the pseudo-inverse of $\underline{J}_{ei}$ and $\underline{J}_{ei}^{\#}$ is a projection into the null-space of $\underline{J}_{ei}$.

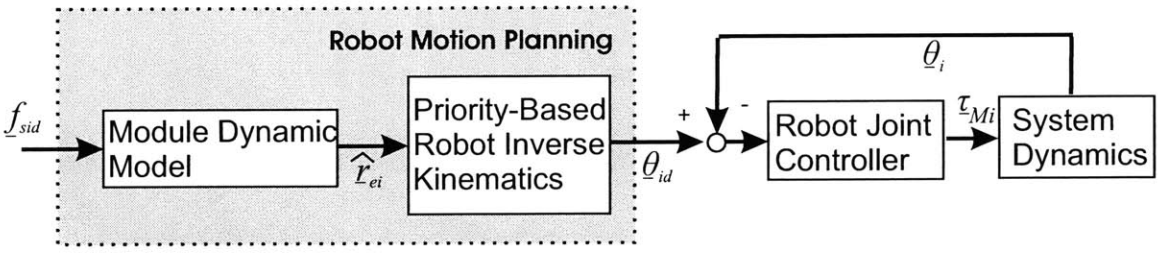

Figure 2.10. Schematic of the robot motion planning and control algorithms of the AMVM.

2.7.2 Robot Motion Control

The first N-2 joints of the robot are controlled by simple joint PD controllers. Since the robot already controls the two components of the force it applies to the module, it cannot control all its joint angles. This is because the robot cannot simultaneously

control the position and the force applied at its end-effector. The output of the PD controller is the joint torque action ${}^{C}\underline{\tau}_{Mi}$:

$$ {}^{C}\underline{\tau}_{Mi} = \underline{K}_{PM}(\underline{\theta}_{id} - \underline{\theta}_{i}) + \underline{K}_{DM}(\dot{\underline{\theta}}_{id} - \dot{\underline{\theta}}_{i}) \tag{2.35} $$

The robot motion controller includes also a feed-forward term ${}^{F}\underline{\tau}_{Mi}$. This feed-forward action can include a friction compensation term, although, in this study the effects of friction were not studied into detail. The total joint torque output $\underline{\tau}_{Mi}$ of the robot motion controller is the sum of the feed-forward action and the joint PD action:

$$ \underline{\tau}_{Mi} = {}^{F}\underline{\tau}_{Mi} + {}^{C}\underline{\tau}_{Mi} \tag{2.36} $$

The response of each robot endpoint depends on the forces $\underline{f}_{si}$ that robots apply to the module. If the inertia properties of the module are poorly known or the tracking errors $\underline{f}_{sid} - \underline{f}_{si}$ are large, then the actual response of the robot endpoint $\underline{r}_{ei}(t)$ will differ significantly from the predicted response $\hat{\underline{r}}_{ei}(t)$. Since the desired joint motions $\underline{\theta}_{id}$ are calculated from $\hat{\underline{r}}_{ei}(t)$, if the deviation $\underline{r}_{ei}(t) - \hat{\underline{r}}_{ei}(t)$ is large, then as the robot motion controller tries to track $\underline{\theta}_{id}$ it affects the motion of the robot endpoint. In this case the robot endpoint controller and the robot motion controller interfere and their performance is degraded. Possible solutions to this problem are to use an impedance controller to compensate the deviation $\underline{r}_{ei}(t) - \hat{\underline{r}}_{ei}(t)$ or to update the desired force profiles $\underline{f}_{sid}$ by an external guidance loop.

2.8 Simulation Results

2.8.1 Simulation Description

This section provides simulation results that demonstrate the effectiveness of the AMVM planning and control architecture. The simulations consider the planar case depicted in Fig. 2.4, where two redundant planar manipulators maneuver a flexible beam into its final desired position. The system is simulated in Matlab/Simulink using the method descried in [13], Fig. 2.11.

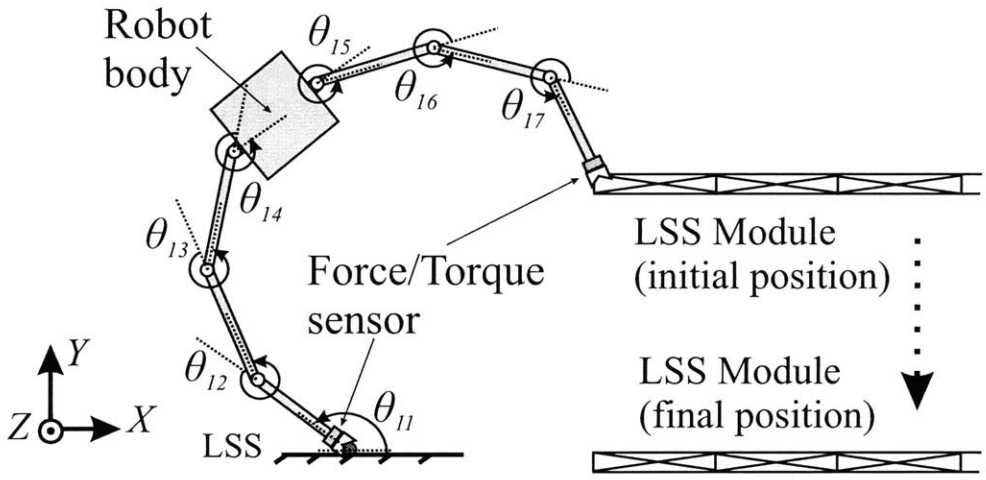

Figure 2.11. The planar system used in simulations. Only one of the two robots is shown.

The properties of the robots are shown in Table 2.2. Each robot has seven links, total length 20 m, total weight 350kg. The mass of the robot is concentrated in its middle link, the robot body. This robot design results in small operational-space inertia which makes easier to control the robot endpoint interaction forces, Section 2.6.4. Each robot has force/torque sensors at its end-effectors. In the simulations of this section robots are assumed to be mounted on a rigid base structure.

Number of links:	7
Link length [m]:	[2.5, 3, 3.5, 2, 3.5, 3, 2.5]
Link mass [kg]:	[10.5,14,14,273,14,14,10.5]

Table 2.2. Robot properties used in the simulations

The module is modelled as an Euler-Bernoulli beam. The properties of the beam considered in the simulations of this section are shown in Table 2.3. The beam initially is at rest.

Length [m]	200
Effective Young's modulus [GPa]	0.159
Linear Density [kg/m]	3
Lowest vibration modes (free-free beam)	f_1=0.197 Hz, f_2=0.539 Hz, f_3=1.042 Hz

Table 2.3. Beam properties used in the simulations

2.8.2 Force Planning

Fig. 2.12 shows results for the force planning algorithm of Section 2.5. All profiles correspond to maneuvering the beam into $\underline{r}_{Gs}(\Delta t) = \begin{bmatrix} 0 & -6 \end{bmatrix}$ and $\theta_s(\Delta t) = 0$. The maneuver duration is Δt=40 sec. The results of the force planning algorithm depend on the range of the angular frequencies ω_{pi} of the sinusoids that are used to create the force profiles $\underline{f}_{sid}$ (Section 2.5). The numerical parameters for each case are shown in Table 2.4. The values of ω_{pi} are found by interpolating $\omega_{pi\max}$ and $\omega_{pi\min}$.

Case	M	$\omega_{pi\max}$ [rad/sec]	$\omega_{pi\min}$ [rad/sec]
1	20	2π/20	2π/80
2	20	2π/10	2π/80
3	20	2π/5	2π/80

Table 2.4. Force planning parameters for the force profiles shown in Fig. 2.12.

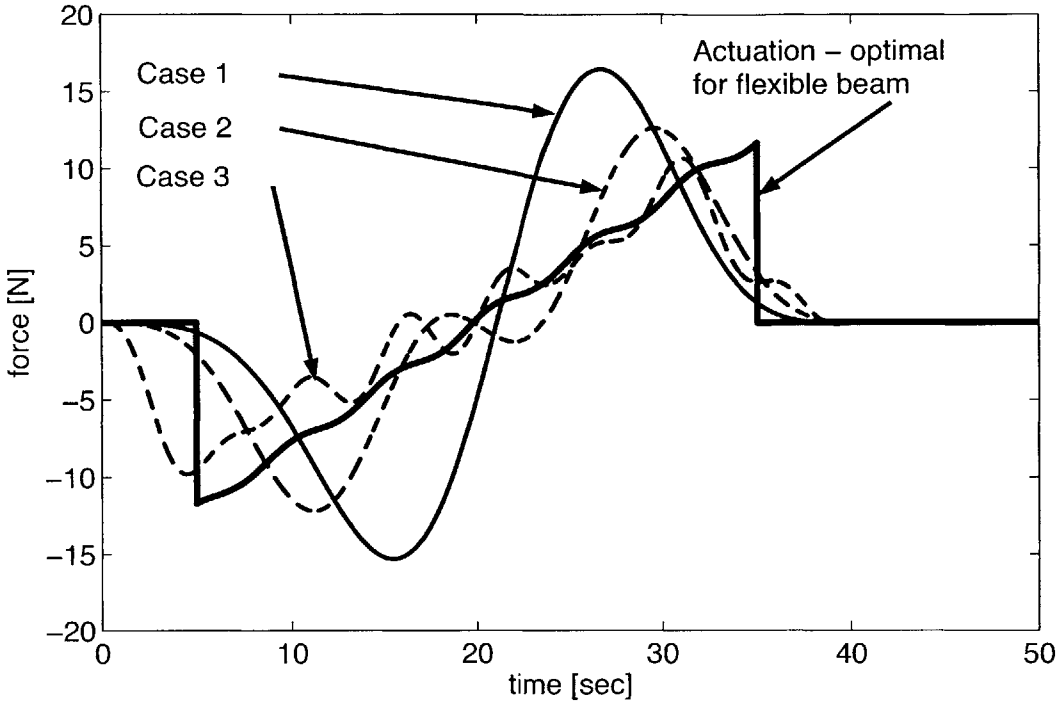

Figure 2.12. Force planning results for various force planning parameters.

Fig. 2.12 also shows the force profile that minimizes the metric $I = \int_0^{\Delta t} \sum_i \left\| \underline{f}_{si} \right\|_2^2 dt$ for a rest to rest motion of the flexible beam [6]. It can be seen that the force profiles $\underline{f}_{sid}$ that are calculated by the planning algorithm of Section 2.5 are always smooth, whereas the theoretical optimal result is not. However, the resulting $\underline{f}_{sid}$ from the force planning algorithm of Section 2.5 are suboptimal with respect to the metric $I = \int_0^{\Delta t} \sum_i \left\| \underline{f}_{si} \right\|_2^2 dt$. It can be seen that as $\underline{f}_{sid}$ are approximated by faster sinusoids (larger $\omega_{pi\max}$) the results tend to the theoretical optimal result. However, as the command signals $\underline{f}_{sid}$ contain faster sinusoids, it is more difficult to track them due to the relative slow bandwidth of the endpoint force controller. The proper force profile is the result of a trade-off between the actuation capabilities of the robot and the limited bandwidth of the endpoint force

controller. It was found that good choices for $\omega_{pi\max}$ and $\omega_{pi\min}$ are $\omega_{pi\max} = \omega_{Fbw}$ and $\omega_{i\min} = \pi/\Delta t$.

Fig. 2.13 shows the response of the beam CM and the vibration in its left end when the force profiles $\underline{f}_{sid}$ that are calculated from the force planning algorithm are applied to the beam as forces. The force profiles are calculated for a 6 m maneuver within 40 sec($\underline{r}_{Gs}(\Delta t) = [0 \quad -6], \theta_s(\Delta t) = 0$, Δt=40 sec, M=20, $\omega_{pi\max}$=2π/15 and $\omega_{pi\min}$=2π/80). This figure shows that beam is positioned accurately to its desired position and with low levels of residual vibration.

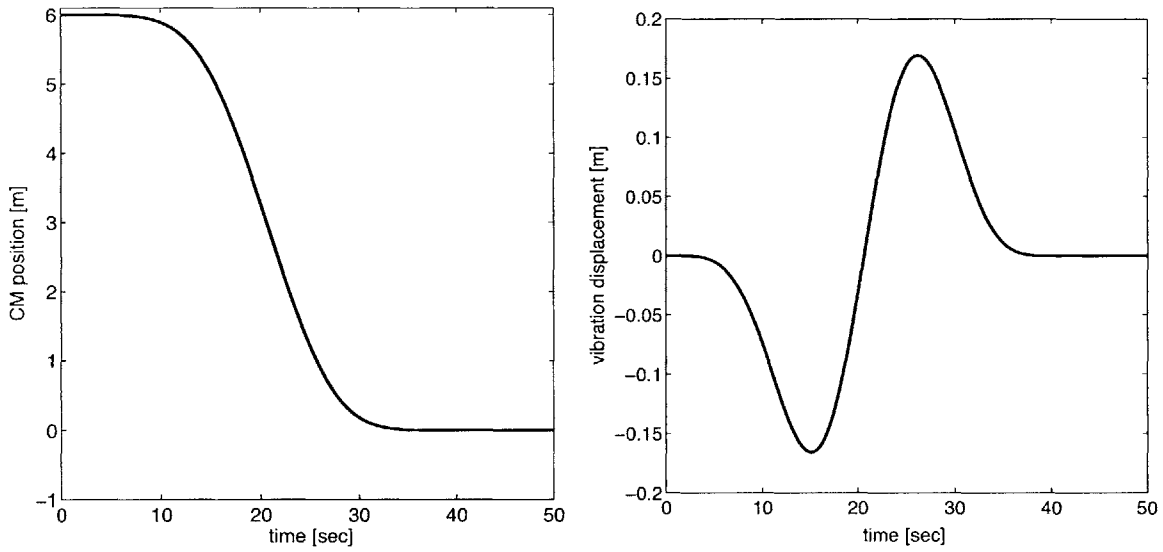

Figure 2.13. Beam CM position and beam end vibration response when the calculated desired endpoint force $\underline{f}_{sid}$ are applied at the ends of the beam (the presence of robots is ignored).

2.8.3 Controller Performance

This section provides simulation results for a sample design of the AMVM architecture. The endpoint force controller consists of a centralized state feedback control action and decentralized PI controllers for each force component, Fig. 2.8. The design of

the centralized controller gain $\underline{K}_F$ is based on a nominal plant of the system, Eq. 2.23, which is calculated considering the first two modes of the free-free beam. The force and torque measurements are filtered by a low-pass filter with cut-off frequency at ω_C=4.5 rad/sec to prevent spillover effects [3]. The gain $\underline{K}_F$ is chosen so that the modified plant $\underline{A}_F^* = \underline{A}_F - \underline{B}_F \cdot \underline{K}_F$ has poles at desired locations of the s plane. The chosen poles of the plant and the modified plant are shown in Table 2.5. The rigid body poles of the system are chosen to lie at s=-0.2 (X motion), s=-0.6 (double pole- Y motion).

Zero of nominal plant (pole of free-free beam)	Desired pole of modified plant
-0.0116 ± 1.1643j	-0.6 ± 0.1j
-0.0321 + 3.2094j	-0.5 ± 2.9j

Table 2.5. Desired poles for the design of the state-space controller.

The decentralized part of the endpoint force controller consists of PI controllers for each component of $\underline{f}_{si}$. The PI controllers G_{CFX}, G_{CFY} that control the X and Y components of $\underline{f}_{si}$ are:

$$G_{CFX} = \frac{0.88s + 0.08}{s^2}$$

$$G_{CFY} = \frac{0.75s + 0.5}{s^2}$$

The PD gains for the first five links are $\underline{K}_{PM}$=1000[38, 22.7, 12, 6, 4] Nm/rad and $\underline{K}_{DM}$=1000[14, 8.4, 7, 6, 4] Nmsec/rad. The active damping added by each robot to the system, Eq 2.32, corresponds to the damping matrix:

$$\underline{D}_{Aid} = \begin{bmatrix} 50 & \\ & 200 \end{bmatrix} \text{ Nsec/m}$$

Fig 2.14 shows the singular value plot of the open loop (Eq. 2.23) and the closed loop dynamics (the dynamics between the command $\underline{f}_{sid}$ and the response $\underline{f}_{si}$). This plot is the generalization of the Bode magnitude diagram for MIMO linear systems [1]. The plot includes only the first two flexible modes of the beam.

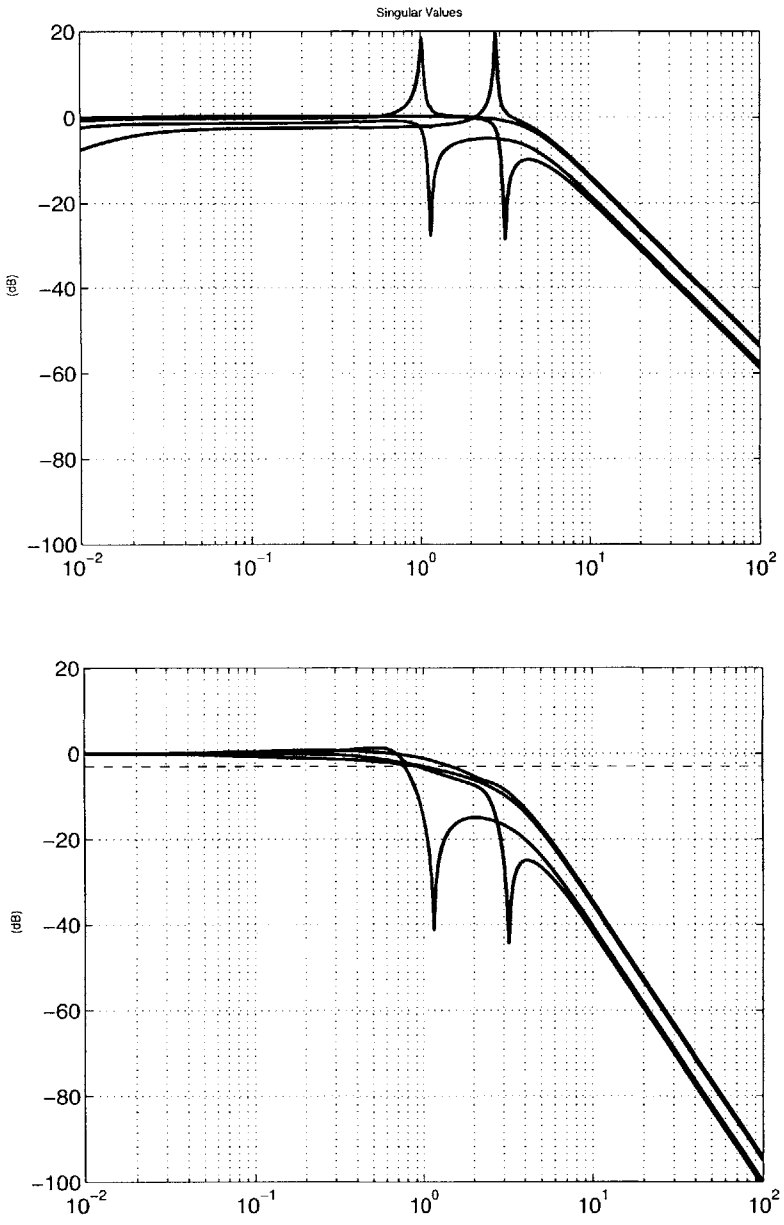

Figure 2.14. Singular values of the open loop (up) and the closed loop dynamics (down) of the robots-module system.

Fig 2.14 shows that the open loop sigma plot has deep notches and high resonant peaks due to the poor damping of the beam. The closed loop sigma plot is smooth and without resonant peaks due to the damping added by the endpoint force controller and the active damping action, Eq. 2.32. The closed loop bandwidth is ω_{Fbw}=0.75 rad/sec since the magnitude of all singular values is larger than -3 dB for $\omega < \omega_{Fbw}$. The maximum closed loop bandwidth that was achieved when each robot controls the force $\underline{f}_{si}$ it exerts to the module independently by PI controllers was ω_{Fbw}=0.25 rad/sec. In that case the robots could not track the forces $\underline{f}_{sid}$ that they need to apply to the module so that they manipulate it within 40 sec. Fig. 2.14 shows that the closed loop bandwidth has deep notches that correspond to the modes of the free-free beam. Therefore, the closed loop bandwidth is limited by the lowest natural frequency of the beam.

The main idea of the AMVM algorithm is to plan and control the forces $\underline{f}_{si}$ that robots apply to the module so that they manipulate it with low levels of residual vibration. Fig 2.15 shows the tracking performance for the force applied by robot 1 to the module. The time lag between the command and the response is less than 1 sec. This lag induces overshoot that is less than 1 N. The controller is able to track the command signal well. The X component of the endpoint force has also overshoot (less than 1 N) even though the desired command here is zero. This shows a dynamic coupling between the X and Y components of the endpoint force which is caused by the non-diagonal mass matrices $\underline{B}_{Ai}$ of the robots.

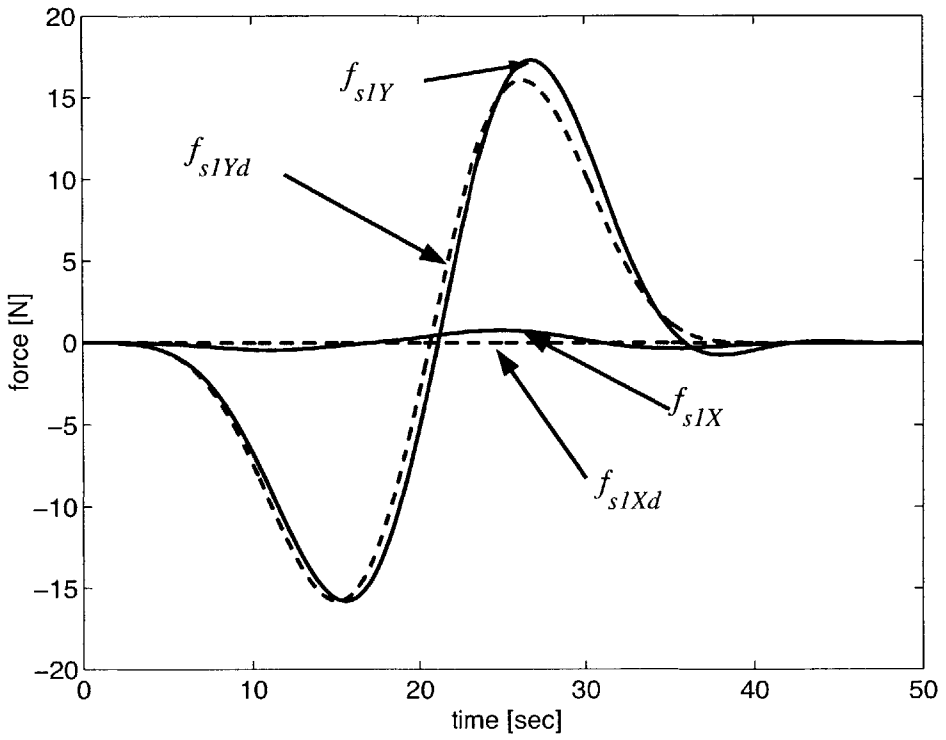

Figure 2.15. Tracking performance for the force applied by robot 1 to the module when the robots use the AMVM architecture.

The endpoint force controller includes a centralized state feedback term that uses measurements of the forces $\underline{f}_{si}$ that robots apply to the module, Fig. 2.8. The communication and process of these signals induces time delays in the system that have not been considered in the results shown in Fig 2.15. Fig 2.16 shows a modification of the endpoint force controller block diagram that presents how such time delays are considered in this study.

Fig 2.17 shows the response of the endpoint force of robot 1 when there is a communication delay of 0.5 sec in the system. The comparison of Fig 2.15 and Fig 2.17 shows that the 0.5 sec delay does not induce major delays and deteriorates the system performance mildly, mainly increasing overshoot. Simulation results show that the system will become unstable when the communication delay is more than 1 sec.

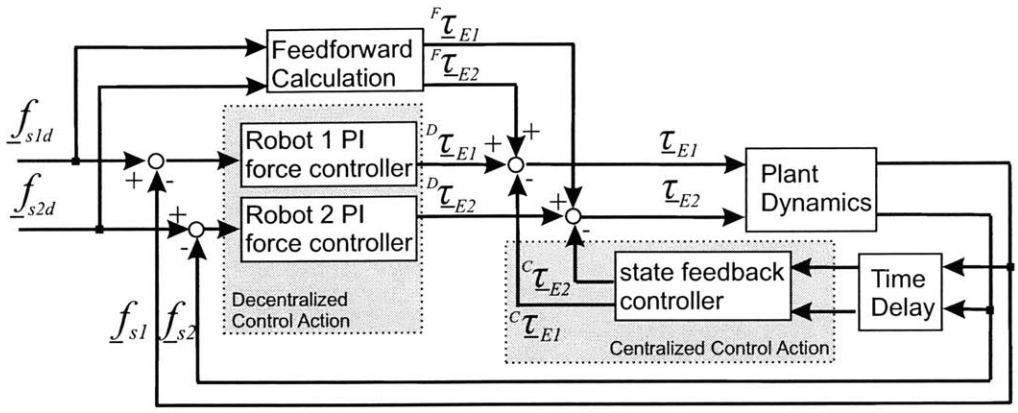

Figure 2.16. Block diagram of the endpoint force controller that includes time delays that take place in the centralized control action.

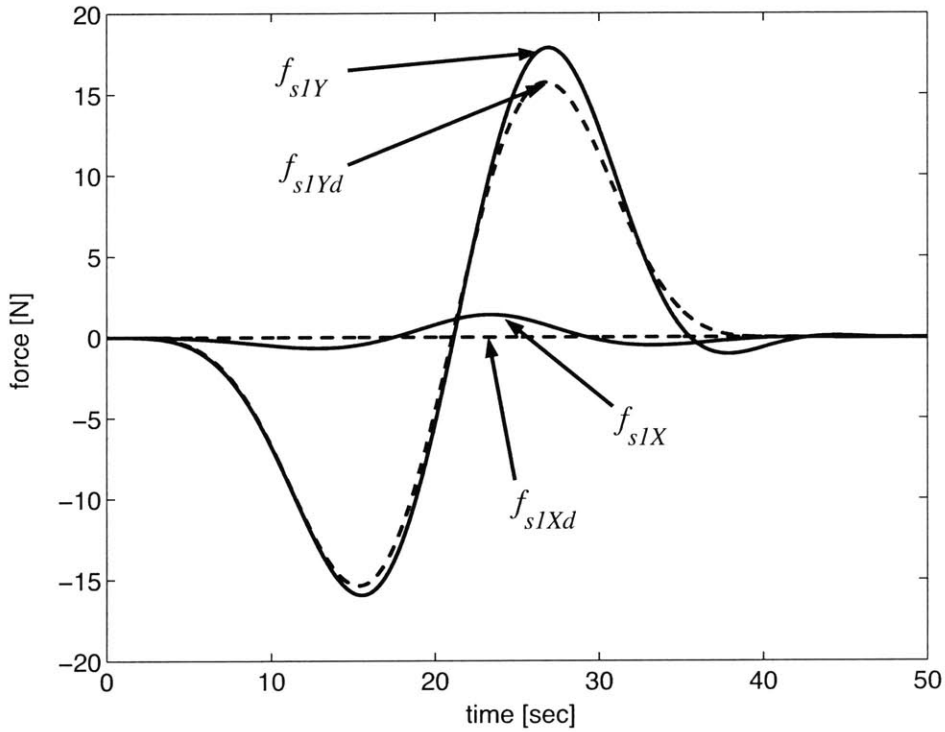

Figure 2.17. Simulation results for the endpoint force of robot 1 in the presence of communication delays (0.5 sec). Robots use the AMVM architecture.

The AMVM makes forces $\underline{f}_{si}$ to track the commanded forces $\underline{f}_{sid}$ well enough to position the beam within the required position accuracy, Table 2.1. Fig. 2.18 shows the beam response using the AMVM architecture and the ideal response of the beam obtained when the beam is driven by forces equal to $\underline{f}_{sid}$. The small tracking errors

$\underline{\tilde{f}}_{si} = \underline{f}_{sid} - \underline{f}_{si}$ induce positioning errors and residual vibration, which however are within the required specifications of Table 2.1.

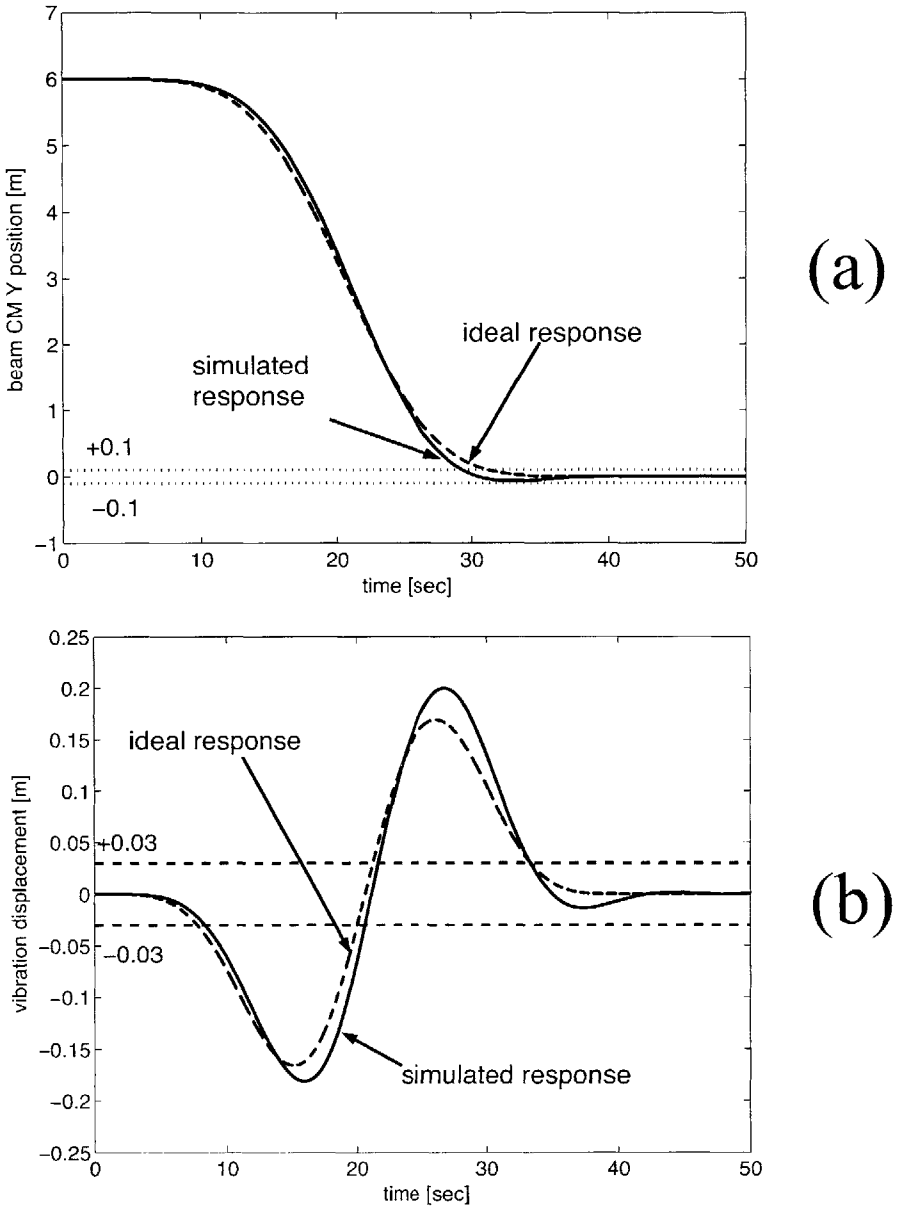

Figure 2.18. Beam CM response (a) and beam left end vibration response (b).

Fig. 2.18a shows the response of the beam CM motion. This figure shows that robots position the beam accurately (the steady state position error is zero) and safely (the

position overshoot is less than 10 cm). Fig. 2.18b shows that the resulting residual vibration in the beam is small and well within the specifications of Table 2.1.

Fig. 2.19 shows the response of the joint angles θ_{1j} of robot 1 and compares them with the command signal θ_{1jd} that is calculated in the robot planning algorithm. This figure shows that the first five joints are controlled accurately (the command and response signals are indistinguishable). The last two joints are not in closed loop position control. The position response of the last two joints is determined by the motion of the beam (and therefore the response of the robot end effector) and the response of the first five robot joints. Fig. 2.19 shows that there is a deviation between the actual and the predicted motion of the last two joint angles. This deviation is caused by the endpoint force tracking errors $\underline{\tilde{f}}_{si}$. This figure also shows that the robot planning algorithm succeeds in avoiding the undesirable robot configurations (the configuration where $|\theta_{16}|$ and $|\theta_{17}|$ are simultaneously below 30 degrees) that can deteriorate significantly the performance of the endpoint force controller, see Section 2.6.4.

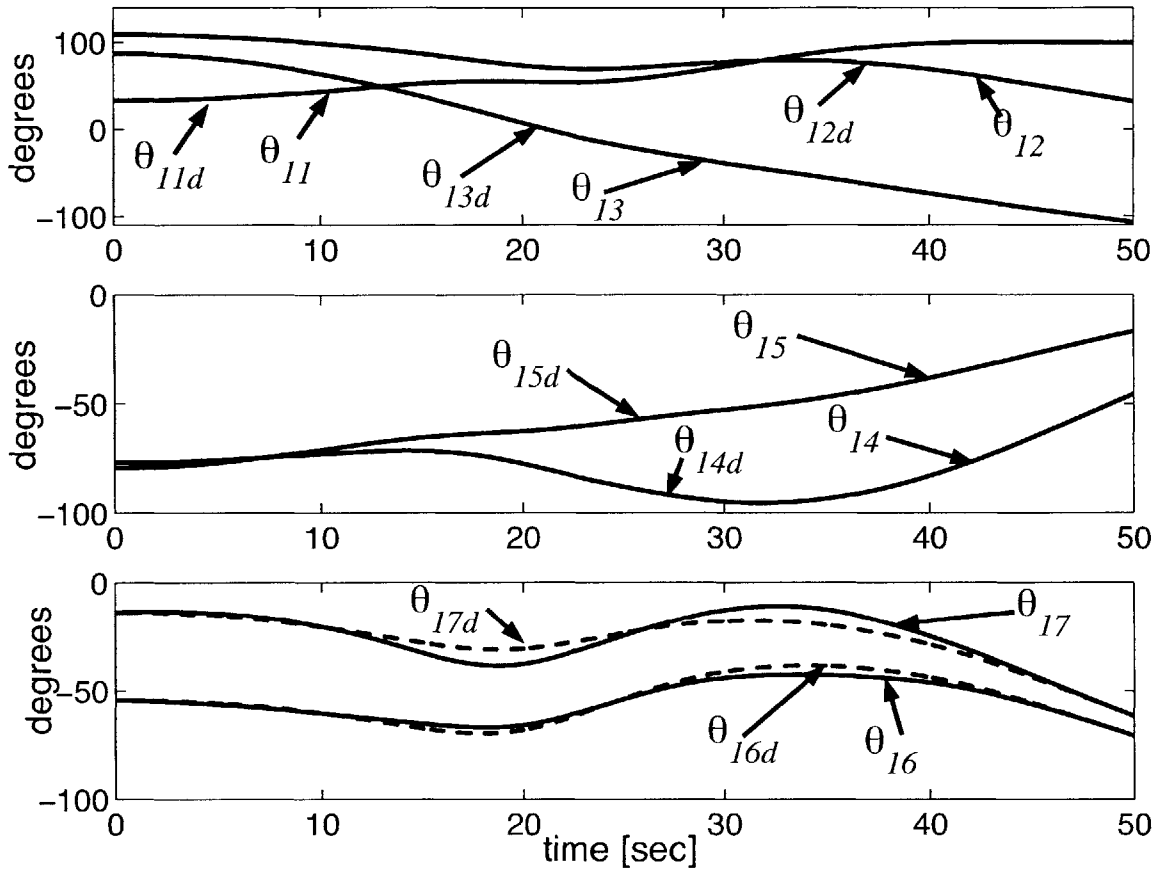

Figure 2.19. Desired joint angles θ_{1jd} and joint angles response θ_{1j} for robot 1. For the first five joint angles of the robot, the two signals are indistinguishable.

Chapter 3
Manipulation of Large Flexible Structures by Robots Mounted on Compliant Bases

3.1 Introduction

Chapter 2 provided a planning and control architecture for the manipulation of a large flexible structure by a team of robots in the proximity of the LSS when the compliance of the LSS is ignored. This chapter expands the architecture to consider the compliance of the robots' base structures. In the architecture developed here, robots plan and control the forces that they apply to both the module and the LSS. Robots still exploit their redundancy to avoid undesirable configurations and obstacles.

The chapter starts by providing a description of the manipulation task and highlighting the effects of the compliance of the LSS. It presents the proposed planning and control architecture, and provides simulation results that demonstrate its effectiveness in positioning the module accurately while inducing small residual vibration in the module and the LSS.

3.2 Task Description

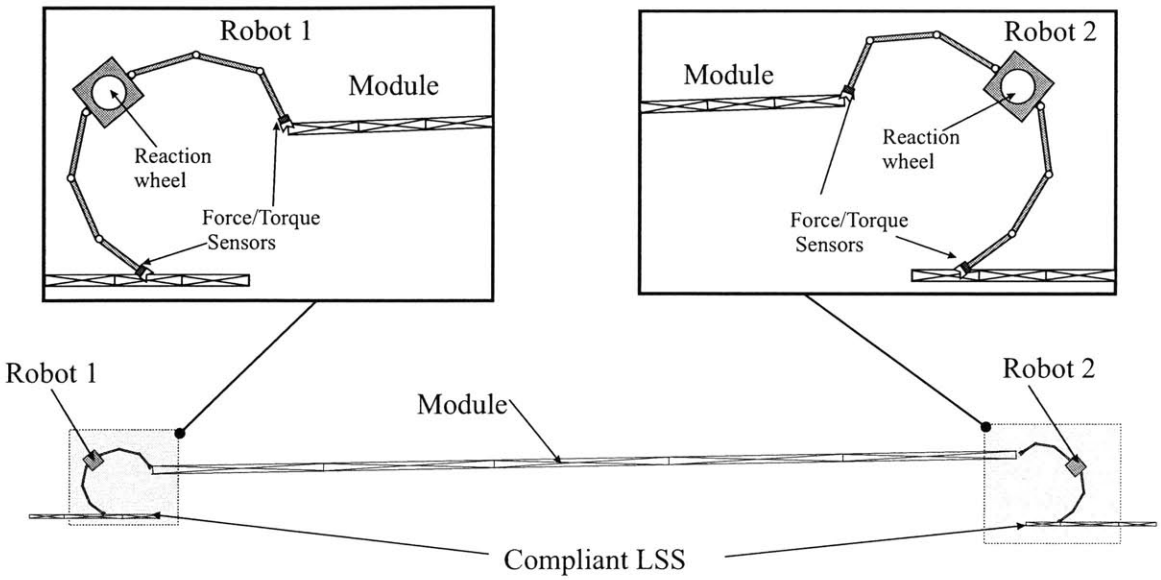

Figure 3.1. Manipulation of a large flexible structural module by a team of robots mounted on the compliant LSS.

Fig. 3.1 shows a representative manipulation task. A large flexible structural module of the LSS, located in the proximity of the LSS, is maneuvered into its pre-assembly position by a team of robots mounted on the LSS. The description of the system with the exception of the compliant base structures was done in section 2.2.

The compliance of the robots' base structures is an important aspect of the problem and should be considered in the analysis. The reaction forces and moments that robots exert to the LSS excite vibration in the LSS. This vibration can have significant amplitude and cause undesirable effects in the system response. Such negative effects are shown in Fig. 3.2 to 3.4. These figures show simulation results for the manipulation of a 200m beam by two 20m robots, which are mounted on compliant base structures. The dynamics of the robot base structure are modeled by a mass-spring system. The natural frequency of the base is 0.1 rad/sec. The robots use the AMVM architecture that was

developed for the case where robots are mounted on a rigid base structure (see Chapter 2).

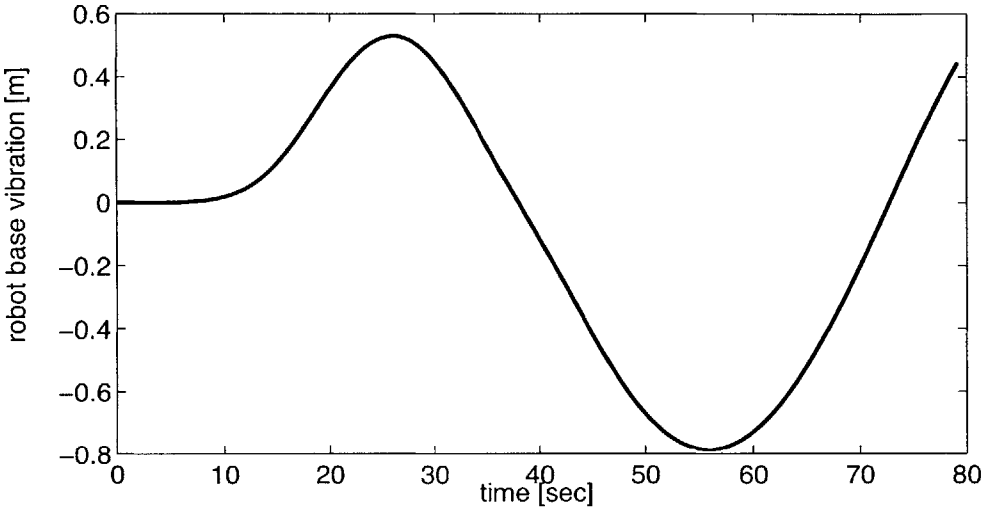

Figure 3.2. Vibration deflection response at the base of robot 1 when the AMVM architecture is applied to robots mounted on compliant structures.

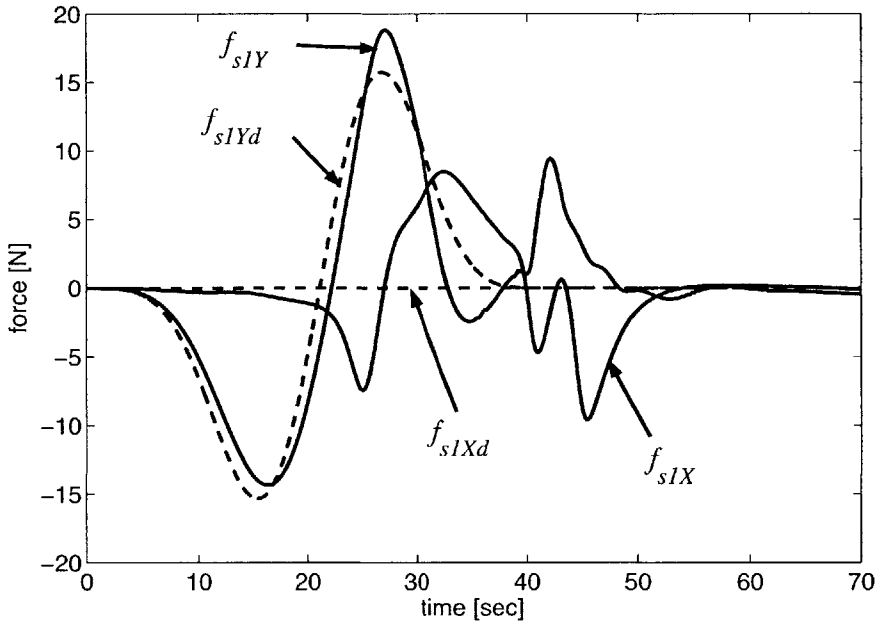

Figure 3.3. Desired force $\underline{f}_{sid}$ and simulation results $\underline{f}_{si}$ when the AMVM architecture is applied to robots mounted on compliant structures.

Fig. 3.2 shows the vibration deflection at the base of robot 1. The base reaction forces are large enough to induce significant deflections in the robots' base structures. This vibration couples with the robot dynamics and can induce significant force tracking errors. This is shown in Fig. 3.3 where the robot fails to control well the forces that it applies $\underline{f}_{si}$ to the module. In this case robots fail to position the module accurately, Fig.3.4. The force tracking errors cause the trajectory of the beam ends to deviate from the desired trajectory. Such positioning errors can result in collisions that could damage the flexible structures and the robots.

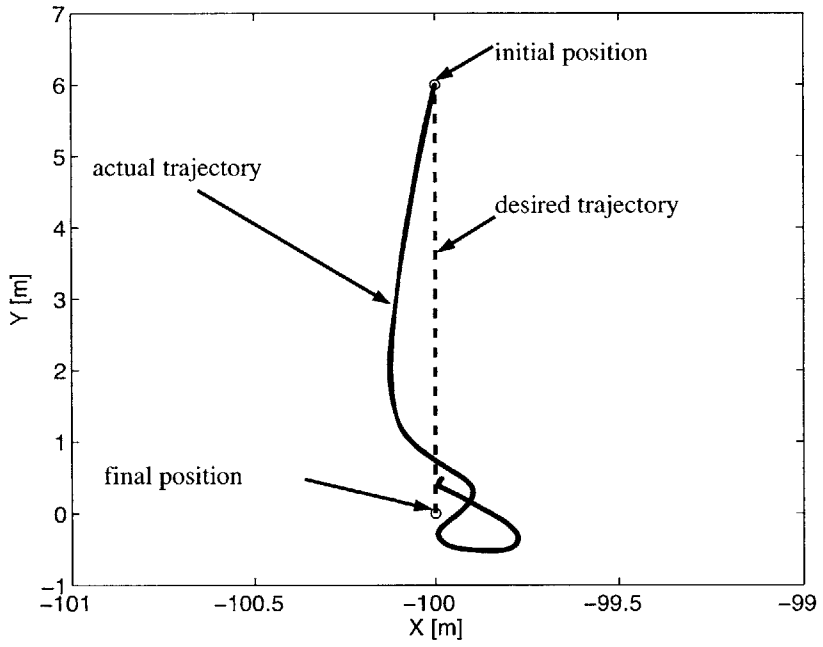

Figure 3.4. Desired and actual trajectory of the left beam end when the AMVM architecture is applied to robots mounted on compliant structures.

Residual vibration in the LSS causes also dimensional mismatch between the mating points of the LSS and the corresponding mating points of the module. These mating points have to be within some distance so that the latching mechanisms, that will connect the module and the LSS, can operate. If significant vibration is induced in the

LSS, robots have to wait for this vibration to damp before they proceed to the next phase of LSS assembly. This results in costly time delays.

In this study it is assumed that initially the LSS is at rest and that there is no outside vibration excitation in the LSS apart from the robots' base reaction forces and moments. Therefore, it is desirable to plan and control the robots so that they manipulate the module into its pre-assembly position accurately while exciting low levels of residual vibration in the module and the LSS. This is achieved by the planning and control architecture described in Sections 3.4 to 3.5.

3.3 System Modeling

A planar model of a representative system considered in this study is shown in Fig. 3.5. Two redundant planar robots manipulate a long flexible module from its initial position in the proximity of the LSS to its pre-assembly position. The robots are mounted on the compliant LSS. While the examples considered in this thesis are planar, the approach can be extended to the general three-dimensional case.

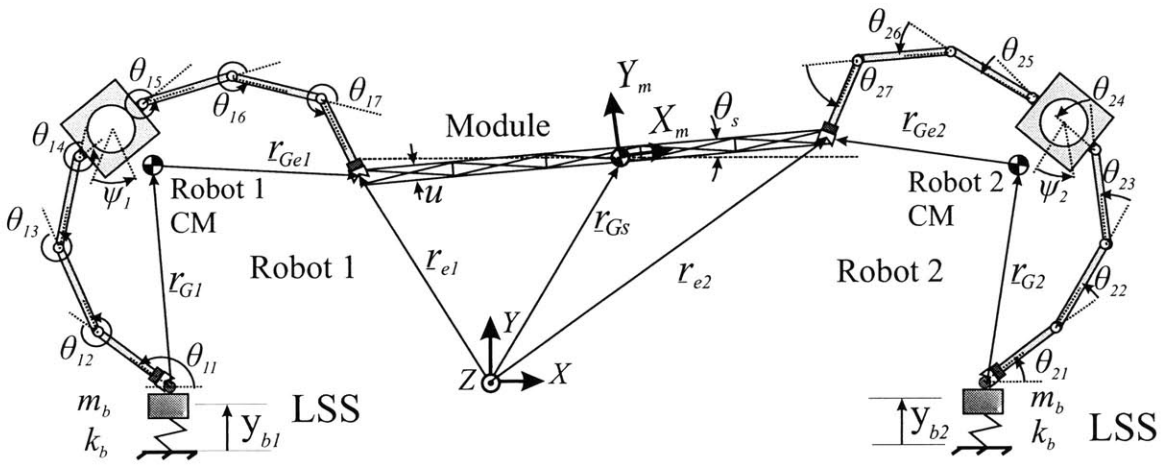

Figure 3.5. Planar model for the manipulation of a large flexible structure by two planar robots mounted on compliant base structures.

The compliance of the module and the robot base structures are important aspects of the task. The large flexible module is modelled as an Euler-Bernouli beam, see section 2.3. Fig. 3.6 shows a sample LSS concept configuration considered in this study. The structure diameter is approximately two kilometers. The stiffness of such a planar-like structure in the plane of the structure is much larger compared to the stiffness in the direction normal to this plane. The dynamic properties of this LSS sample configuration were analyzed using finite element analysis. The complete structure is made of 420 beam-like structural modules (Fig 2.5). The total weight of the LSS is about 250 tn. The period of the structure's lowest mode is about 10.4 min.

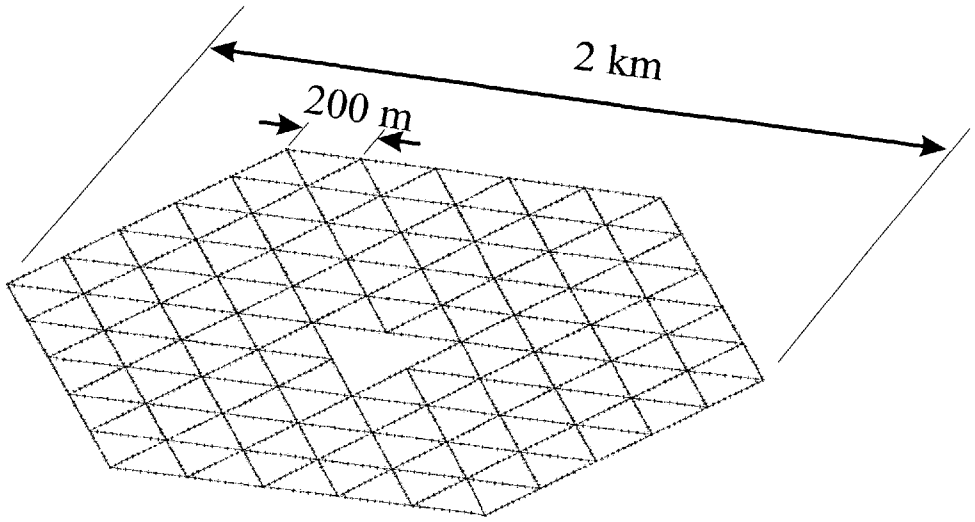

Figure 3.6. Example LSS concept configuration considered in the study.

Each robot is assumed to have N rigid links (where N>2 so that it is redundant with respect to positioning its end-effector at inertial position $\underline{r}_{ei}$) and a reaction wheel whose axis is parallel to the inertial Z axis, Fig. 3.5. Each robot firmly grasps the module and the connection acts as a pinned joint. The configuration of each robot is described by the vector $\underline{\vartheta}_i$ that contains the robot joint angle vector $\underline{\theta}_i$ and the angular position of its reaction wheel ψ_i (subscript i = 1 refers to the left robot and i = 2 to the right robot):

$$\underline{\vartheta}_i = \begin{bmatrix} \underline{\theta}_i^T & \psi_i \end{bmatrix}^T, \quad i = 1, 2 \tag{3.1}$$

Here, it is assumed that the XZ plane coincides with the plane of the LSS shown in Fig. 3.6. Therefore, each robot base is assumed to be rigid in the X direction and compliant in the Y direction. The dynamics of the LSS in the Y direction are modeled by a mass m_B and a spring rate k_B. This model assumes that base reaction forces/moments of each robot do not induce vibration in the base structure of the other robots of the team. The dynamics of each robot (including the effects of its base structure) are:

$$\begin{bmatrix} \underline{B}_i & m_{Ri}\underline{J}_{Gi}^T \\ m_{Ri}\underline{J}_{Gi} & m_{Ri}+m_B \end{bmatrix}\begin{bmatrix} \ddot{\underline{\vartheta}}_i \\ \ddot{y}_{bi} \end{bmatrix} + \underline{\eta}_i^* + \begin{bmatrix} 0 & 0 \\ 0 & k_B \end{bmatrix}\begin{bmatrix} \underline{\vartheta}_i \\ y_{bi} \end{bmatrix} = \begin{bmatrix} \underline{\tau}_i \\ 0 \end{bmatrix} - \begin{bmatrix} \underline{J}_{ei}^T(\underline{\theta}_i) \\ 1 \end{bmatrix}\underline{f}_{si} \tag{3.2}$$

where y_{bi} is the vibration displacement of the robot base in the Y direction, $\underline{\eta}_i^*$ are nonlinear terms, m_{Ri} is the total mass of robot i, and $\underline{J}_{Gi}$ is a Jacobian matrix for the motion of the robot CM with respect to its base:

$$\dot{\underline{r}}_{Gi} = \underline{J}_{Gi}(\underline{\vartheta}_i)\dot{\underline{\vartheta}}_i \tag{3.3}$$

Using Newton laws, the base reaction forces $\underline{f}_{bi}$ and moments $\underline{\mu}_{bi}$ that each robot applies to the LSS are:

$$\begin{bmatrix} \underline{f}_{bi} \\ \underline{\mu}_{bi} \end{bmatrix} = -\frac{d}{dt}\begin{bmatrix} \underline{L}_i \\ \underline{H}_i \end{bmatrix} - \begin{bmatrix} \underline{f}_{si} \\ \underline{r}_{Gei} \times \underline{f}_{si} - \underline{r}_{Gi} \times \underline{f}_{bi} \end{bmatrix} \tag{3.4}$$

where $\underline{L}_i$, $\underline{H}_i$ are the robot's linear and angular momentum, and $\underline{r}_{Gei}$ is a vector that starts at the robot CM and ends at its end-effector. Assuming that the motion of the robot base structure $\dot{y}_{bi}$ is slow compared to the motion of the robot joints, then the robot momentum is approximated as a function of its state $\underline{\vartheta}_i$ by a Jacobian matrix $\underline{J}_{Ri}(\underline{\vartheta}_i)$:

$$\begin{bmatrix} \underline{L}_i \\ \underline{H}_i \end{bmatrix} = \underline{J}_{Ri}(\underline{\vartheta}_i)\dot{\underline{\vartheta}} = \underline{J}_{Ri}(\underline{\vartheta}_i)\begin{bmatrix} \dot{\underline{\theta}}_i \\ \dot{\underline{\psi}}_i \end{bmatrix} \tag{3.5}$$

3.4 Planning and Control Architecture Overview

This section describes the developed planning and control architecture for the manipulation of a large flexible structural module by robots mounted on a compliant LSS. The essential idea of the planning and control architecture is to divide the whole

system into subsystems (robots, module, robot base structures) and control the interaction forces between these subsystems. These interaction forces are the forces $\underline{f}_{si}$ that robots apply to the module, and the base reaction forces $\underline{f}_{bi}$ and moments $\underline{\mu}_{bi}$ that robots apply to the LSS.

Fig. 3.7 shows the block diagram of the planning and control architecture (Architecture for Minimum Vibration Interaction – AMVI). Robots plan and control cooperatively the forces $\underline{f}_{si}$ that they apply to the beam so that the beam is positioned accurately and with low levels of residual vibration. Robots also regulate to zero the components of their base reaction forces $\underline{f}_{bi}$ and moments $\underline{\mu}_{bi}$ that induce significant vibration in their base. At the same time they exploit their redundancy to avoid undesirable configurations and obstacles. Robots are able to control the forces they apply to the flexible structures by using force/torque sensors at their endpoints. Robots also improve their ability to control base reaction moments $\underline{\mu}_{bi}$ by using reaction wheels.

In the AMVI architecture, the total joint torque output for each robot $\underline{\tau}_i$ is the sum of the joint torque output of the endpoint force controller $\underline{\tau}_{Ei}$ and the joint torque output of the robot base reaction force/moment controller $\underline{\tau}_{Bi}$.

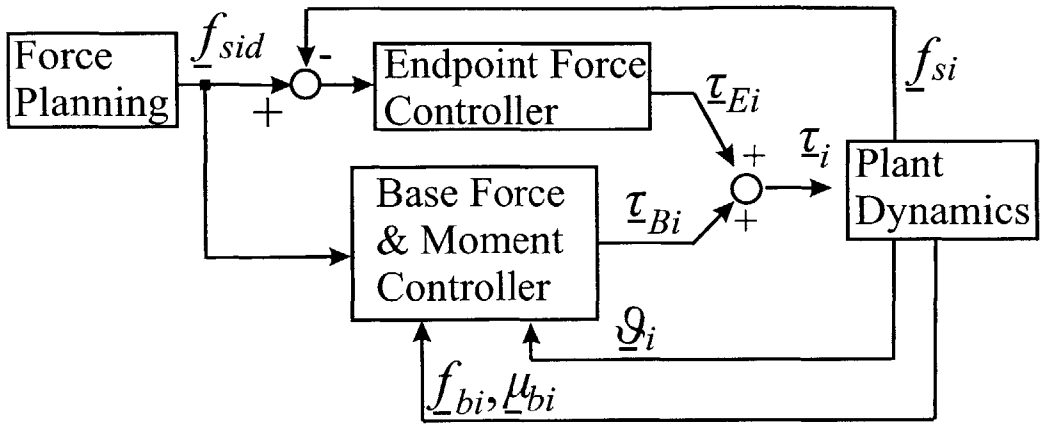

Figure 3.7. Overview of the Architecture for Minimum Vibration Interaction (AMVI).

The AMVI architecture is an extension of the AMVM architecture that was developed for the manipulation of large flexible structures by robots that are mounted on a rigid base structure, see Chapter 2. In AMVM robots plan and control only the interaction forces $\underline{f}_{si}$ they apply to the module. In AMVI robots plan and control cooperatively the forces $\underline{f}_{si}$ the same way as in AMVM. The force planning and control algorithms for the endpoint forces $\underline{f}_{si}$ are described in Chapter 2. In AMVI robots also exploit their redundancy to plan and control individually the base reaction forces $\underline{f}_{bi}$ and moments $\underline{\mu}_{bi}$ that they apply to the LSS. The force control action on $\underline{f}_{bi}$ and $\underline{\mu}_{bi}$ is implemented indirectly, by proper planning and control of the robot redundant degrees of freedom (redundant links and reaction wheels).

The design of the robot controllers is based on the assumed set of specifications shown in Table 3.1. The parameters $\delta \underline{r}_{Gs}$, $\delta\theta_s, \delta u_{tip}$ have been defined in Section 2.4. δy_{bi} is the maximum allowable residual vibration in the base structure of each robot.

Beam position error of $\delta \underline{r}_{Gs}(\Delta t)$	[m]	± 0.10
Beam orientation error $\delta\theta_s(\Delta t)$	[deg]	± 0.05
Residual vibration in beam ends δu_{tip}	[m]	± 0.03
Residual vibration in the LSS δy_{bi}	[m]	± 0.05

Table 3.1. Specifications for the design of the AMVI planning and control architecture.

3.5 Base Reaction Force/Moment Control

3.5.1 Base Reaction Force/Moment Controller Overview

This study assumes that initially the LSS is at rest. It is desirable to keep LSS vibration small (and therefore the vibration of the robots' base structures) by eliminating the components of robot base reaction forces $\underline{f}_{bi}$ and moments $\underline{\mu}_{bi}$ that induce significant vibration in the LSS. The objective of the robot base reaction force/moment controller is to regulate these components of $\underline{f}_{bi}$ and $\underline{\mu}_{bi}$ to zero. Additionally, the robot base reaction force/moment controller exploits robot redundancy to avoid undesirable configurations and joint limits.

For the planar example considered in this study, Fig 3.5, it is assumed that the XZ inertial plane coincides with the plane of the sample LSS configuration shown in Fig. 3.6. Therefore it is desired that each robot eliminates the component of is base reaction force $\underline{f}_{bi}$ that is parallel to the Y axis.

The implementation of the base reaction force/moment controller is different than the implementation of the endpoint force controller (Section 2.6). The base reaction force/moment controller regulates the components of interest of $\underline{f}_{bi}$ and $\underline{\mu}_{bi}$ indirectly, by planning and control the robot redundant degrees of freedom. For the planar case

considered here, each robot already controls the two components of the force $\underline{f}_{si}$ that it applies to the module. Therefore, the redundant degrees of freedom of each robot are its first N-2 joint angles ($\theta_{i,1}$ to $\theta_{i,N-2}$) and the angular position of its reaction wheel ψ_i.

Fig. 3.8 shows the block diagram of the base reaction force/moment controller. The comparison of Fig. 3.8 and 2.10 shows that the base reaction force/moment controller is an extension of the robot motion planning and control algorithm that is used in the AMVM architecture, Section 2.7.

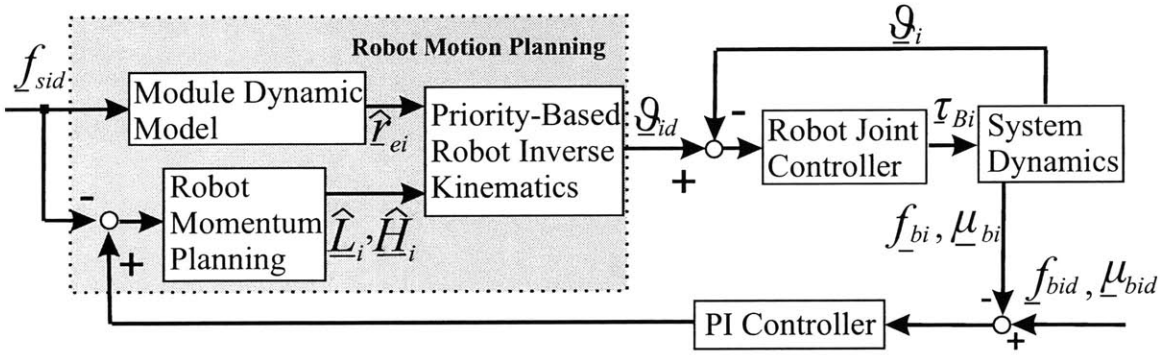

Figure 3.8. Base reaction force/moment controller.

The base reaction force/moment controller consists of an outer force feedback loop that modifies the commands of an inner position control loop. Therefore, it can be considered as a variation of the parallel force/position control scheme [8]. The inner position control loop consists of PD controllers for each robot redundant degree of freedom. The commands for this inner control loop (the desired motion of the robot redundant joint angles $\underline{\theta}_{id}$ and the desired angular position $\underline{\psi}_{id}$ of the robot reaction wheel) are calculated by the robot motion planning algorithm. The outer control loop modifies the input of the robot motion planning algorithm as a function of force tracking

errors $\underline{\tilde{f}}_{bi} = \underline{f}_{bid} - \underline{f}_{bi}$ and $\underline{\tilde{\mu}}_{bi} = \underline{\mu}_{bid} - \underline{\mu}_{bi}$ through PI controllers, Fig. 3.8. Here, the desired base reaction forces and moments are $\underline{f}_{bid} = \underline{\mu}_{bid} = 0$ (for the components of interest).

3.5.2 Robot Motion Planning

The desired motion of the robot joints $\underline{\theta}_{id}$ and the robot reaction wheel ψ_{id} are calculated by a priority-based inverse kinematics algorithm [26]. The first priority of the algorithm is that the desired robot motion should be compatible with a prediction of the motion $\underline{\hat{r}}_{ei}(t)$ of the corresponding beam end:

$$\underline{J}_{tei}\begin{bmatrix}\dot{\underline{\theta}}_{id}\\ \dot{\psi}_{id}\end{bmatrix} = \dot{\underline{\hat{r}}}_{ei} \tag{3.6}$$

$$\underline{J}_{tei} = \begin{bmatrix}\underline{J}_{ei} & 0\end{bmatrix} \tag{3.7}$$

The second priority of the robot motion planning algorithm is to exploit robot redundancy to eliminate the components of interest of the robot base reaction forces $\underline{f}_{bi}$ and moments $\underline{\mu}_{bi}$. This is done in a modelled-based way by approximating the robot linear momentum $\underline{L}_i$ and angular momentum $\underline{H}_i$ as a function of the robot generalized coordinates:

$$\begin{bmatrix}\underline{\hat{L}}_i\\ \underline{\hat{H}}_i\end{bmatrix} = \underline{\hat{J}}_{Ri}\begin{bmatrix}\dot{\underline{\theta}}_i\\ \dot{\psi}_i\end{bmatrix} \tag{3.8}$$

where $\underline{\hat{J}}_{Ri}$ is a computationally efficient Jacobian matrix that approximates $\underline{J}_{Ri}$ (Section 3.3). According to Newton's law, the base reaction forces and moments of all robots are

eliminated if the total momentum of the robots-module system is kept constant and if the momentum of each robot varies according to Eq. 3.4 when $\underline{f}_{bi} = \underline{\mu}_{bi} = 0$:

$$\frac{d}{dt}\begin{bmatrix}\underline{L}_i \\ \underline{H}_i\end{bmatrix} = -\begin{bmatrix}\underline{f}_{si} \\ \underline{r}_{Gei} \times \underline{f}_{si} - \underline{r}_{Gbi} \times \underline{f}_{bi}\end{bmatrix} \tag{3.9}$$

The right side of Eq. 3.9 contains the effective forces and moments at the robot CM due to the force $-\underline{f}_{si}$ applied by the module to the robot. The robot motion is planned so that the estimated robot momentum (Eq. 3.8) varies according to Eq. 3.9 when $\underline{f}_{si}$ is approximated by $\underline{f}_{sid}$:

$$\hat{\underline{J}}_{Ri}\begin{bmatrix}\dot{\underline{\theta}}_{id} \\ \dot{\psi}_{id}\end{bmatrix} = \int_0^t \begin{bmatrix}-\underline{f}_{sid} + \underline{f}_{BCL} \\ -\underline{r}_{Gei} \times \underline{f}_{sid} + \underline{\mu}_{BCL}\end{bmatrix} d\varsigma + \begin{bmatrix}\hat{\underline{L}}_i(0) \\ \hat{\underline{H}}_i(0)\end{bmatrix} \tag{3.10}$$

It is assumed that initially the robot is at rest, so $\hat{\underline{L}}_i(0) = \hat{\underline{H}}_i(0) = 0$. The vector $\underline{f}_{BCL}$ contains the outputs of the PI controllers of the outer control loop due to errors in base reaction forces $\tilde{\underline{f}}_{bi} = \underline{f}_{bid} - \underline{f}_{bi} = -\underline{f}_{bi}$. The vector $\underline{\mu}_{BCL}$ contains the outputs of the PI controllers of the outer control loop due to errors in base reaction moments $\tilde{\underline{\mu}}_{bi} = \underline{\mu}_{bid} - \underline{\mu}_{bi} = -\underline{\mu}_{bi}$:

$$\begin{bmatrix}\underline{f}_{BCL} \\ \underline{\mu}_{BCL}\end{bmatrix} = \underline{G}_{BF}(s)\left\{\begin{bmatrix}\tilde{\underline{f}}_{bi} \\ \tilde{\underline{\mu}}_{bi}\end{bmatrix}\right\} \tag{3.11}$$

where $\underline{G}_{BF}(s)$ is a diagonal transfer matrix. Each diagonal element of $\underline{G}_{BF}(s)$ is the PI controller for the corresponding component of the robot base reaction forces or moments.

The third priority of the inverse kinematics algorithm exploits robot redundancy to avoid undesirable configurations and obstacles. This is achieved by planning $\underline{\theta}_{id}$ to minimize a smooth potential function $W(\underline{\theta}_i)$ [18]. The resulting desired motion of the inverse kinematics algorithm is [26]:

$$\begin{bmatrix} \dot{\underline{\theta}}_{id} \\ \dot{\psi}_{id} \end{bmatrix} = \underline{J}^{+}_{tei}\dot{\hat{\underline{r}}}_{ei} + \underline{J}^{\#}_{tei}(\hat{\underline{J}}_{Ri}\underline{J}^{\#}_{tei})^{+}(\int_0^t \begin{bmatrix} -\underline{f}_{sid} + \underline{f}_{BCL} \\ -\underline{r}_{Gei}\times\underline{f}_{sid} + \underline{\mu}_{BCL} \end{bmatrix} d\sigma - \hat{\underline{J}}_{Ri}\underline{J}^{+}_{tei}\dot{\hat{\underline{r}}}_{ei}) - \\ -\underline{J}^{\#}_{tei}(\hat{\underline{J}}_{Ri}\underline{J}^{\#}_{tei})^{+}(\frac{\partial W}{\partial \underline{\theta}_i}\Big|_{\underline{\theta}_{id}})^{T} \tag{3.12}$$

where the subscript "+" denotes the pseudo-inverse of a matrix and the subscript "#" denotes a projection into the null-space of a matrix.

3.5.3 Workspace Limitations

In the AMVI architecture each robot controls the forces $\underline{f}_{si}$ that it applies to the module and the forces $\underline{f}_{bi}$ and moments $\underline{\mu}_{bi}$ that it applies to the LSS. This is possible as long as the robot can vary its linear momentum according to Eq. 3.9. Assuming that the motion of the robot base is slow, the robot momentum is approximated as:

$$\underline{L}_i = -m_{Ri}\dot{\underline{r}}_{Gi} \tag{3.13}$$

where $\underline{r}_{Gi}$ is the position of the robot CM position relative to its base. Therefore, the ability of the robot to apply the AMVI architecture is limited by the finite size of the locus of reachable locations for the robot CM $\underline{r}_{Gi}$ (CM-workspace). If the robot CM-workspace is large, the robot can apply larger forces (which cause higher acceleration $\ddot{\underline{r}}_{Gi}$) for larger time duration without violating the CM-workspace limitation. This makes

the robot able to manipulate larger modules for longer distances without exerting base reaction forces and moments.

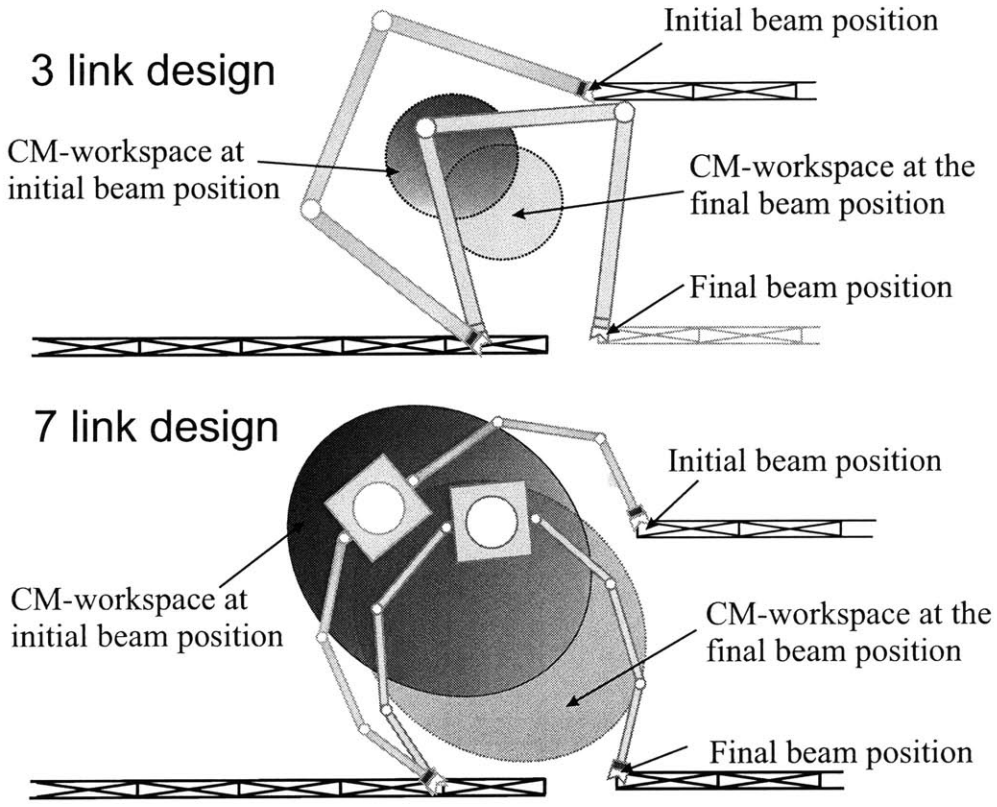

Figure 3.9. CM workspace for two robot designs (of same total mass and length) at the beginning and the end of the manipulation task.

Fig. 3.9 compares the size of the CM-workspace of two robot designs that have the same total mass and total length. The first design is a three-link robot whose weight is evenly distributed along its length. The second design is a seven-link robot whose weight is concentrated in a central heavy body. The seven-link design has significantly larger CM-workspace. For this design, the robot CM is located near the robot body CM. The large number of links makes this robot able to position its body (and therefore its CM) inside a large area for the same end-effector position $\underline{r}_{ei}$.

The application of the AMVI can be improved by using reaction wheels to control the robot's base reaction moments. Reaction wheels do not have workspace constraints. Their performance is limited only by actuator torque and speed limits.

3.6 Results

3.6.1 Simulation Description

This section provides simulation results that demonstrate the effectiveness of the planning and control method described in Fig 3.7. The simulations consider the planar case depicted in Fig. 3.5. Each robot has seven links, total length 20 m, total weight 350kg and its mass is concentrated in its middle link (the robot body). Each robot has force/torque sensors at its end-effectors and a reaction wheel at its middle link, see Fig. 3.10. The beam has length 200 m and total mass 600 kg. Section 2.8.1 provides more information about the properties of the robots and the beam. The system is simulated in Matlab/Simulink using the method described in [13].

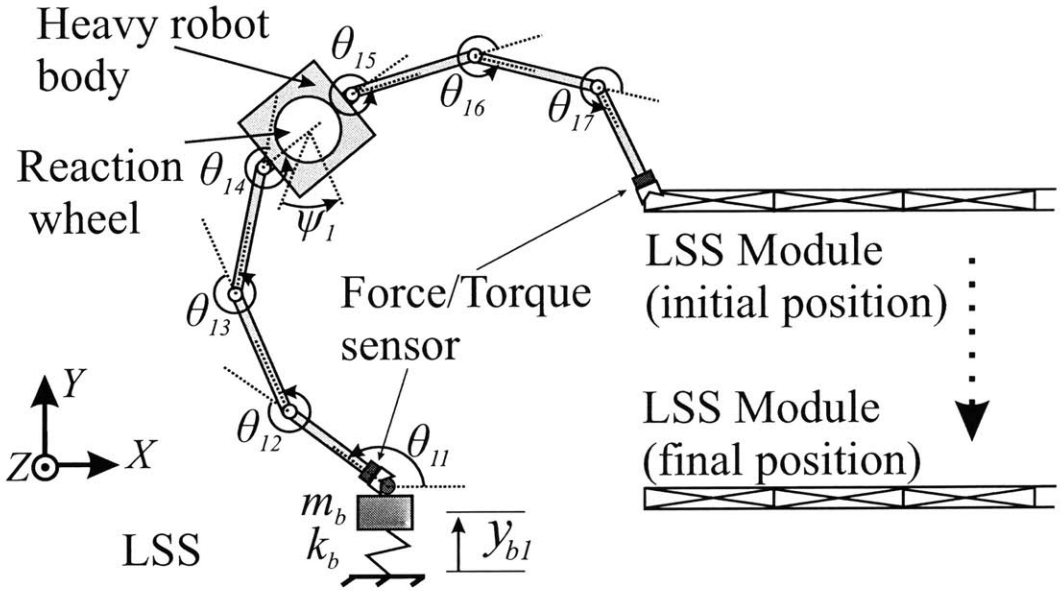

Figure 3.10. The planar system used in simulations. Only one of the two robots is shown.

The robot base structure is considered rigid in the X direction and compliant in the Y direction. The base dynamics in the Y direction are modelled by a mass m_B of 2000 kg and a spring rate k_B of 20 N/m, Fig. 3.10. The natural frequency of the base dynamics is 0.1 rad/sec.

The seven-link robot design used in the simulations has two desirable characteristics. The low inertia with respect to its operational space (see Section 2.8.1) enhances its ability to control the forces $\underline{f}_{si}$ that it applies to the module. The large CM-workspace (a circle of about 9m radius) enhances its ability to eliminate its base reaction forces and moments while it manipulates large flexible modules.

3.6.2 Controller Performance

This section provides simulation results for a sample controller design. The design of the endpoint force controller is the same as the design described in Section 2.8.3. For the planar case considered here the base is assumed to be rigid in the X direction. Each robot needs to regulate only the Y component of its base reaction force. Each robot reduces the magnitude of its base reaction moment by planning the motion of its joints and its reaction wheel, Section 3.5.2. In the general three dimensional case, robots can control all the reaction components of $\underline{f}_{bi}$ and $\underline{\mu}_{bi}$.

The gains of the PD joint controllers for the first five links of the robots are $\underline{K}_{PM}$=1000[38, 22.7, 12, 6, 4] and $\underline{K}_{DM}$=1000[14, 8.4, 7, 6, 4]. The gains for the PD joint controller of the reaction wheel are k_{Pw}= 200 and k_{Dw}= 500. These position

controllers implement the inner control loop of Fig. 3.8. The PI controller for the Y component of the base reaction force is (outer control loop of Fig. 3.8):

$$G_{BF}(s) = 1 + \frac{1}{s}$$

The dynamics of the $G_{BF}(s)$ controller are one order of magnitude faster than the dynamics of the base.

The calculation of the Jacobian $\underline{\hat{J}}_{Ri}$ that approximates the momentum of the robot is based on the linear and angular velocity of the robot body (heavy middle link) and the reaction wheel.

The simulation results of this section, correspond to a maneuver of 6 m in the Y axis within 40 seconds. The desired forces $\underline{f}_{sid}$ that robots need to apply to the beam are calculated from the force planning algorithm of Section 2.5 for $\underline{r}_{Gs}(\Delta t) = [0 \quad -6], \theta_s(\Delta t) = 0$, Δt=40 sec, M=20, $\omega_{pi\max}$=2π/15 and $\omega_{pi\min}$=2π/80.

Fig. 3.11 and 3.12 demonstrate the effectiveness of the AMVI architecture in eliminating the base reaction forces and moments of robots that are mounted on compliant base structures. They show simulation results using the AMVI architecture (developed for robots mounted on compliant base structures - Chapter 3) and simulation results using the planning AMVM architecture (developed for robots mounted on rigid base structures - Chapter 2).

Fig. 3.11 shows simulation results for the Y component of the base reaction force f_{b1Y} of robot 1. AMVM does not control the base reaction forces of the robots. In this case, the maximum magnitude of the base reaction forces is on the same order of

magnitude as the command $\underline{f}_{sid}$ for this robot. On the other hand, the closed loop control action of AMVI managed to regulate the Y component of the robot base reaction forces and keep it below 3 N.

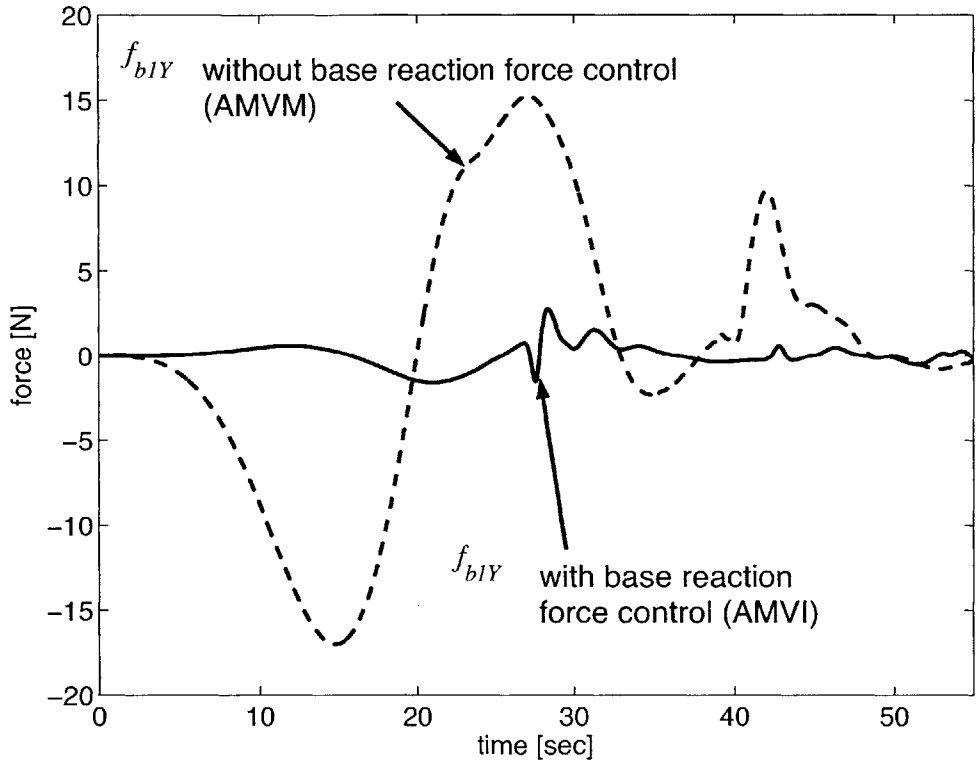

Figure 3.11. Simulation results for the Y component of robot 1 base reaction force with and without base reaction force control action.

Fig. 3.12 shows simulation results for the base reaction torque of robot 1. This reaction component is not controlled in closed loop because it is a control input for the robot controller itself. However, Fig. 3.12 shows that AMVI reduced the magnitude of the base reaction moment by proper planning and control of the motion of the robot reaction wheel.

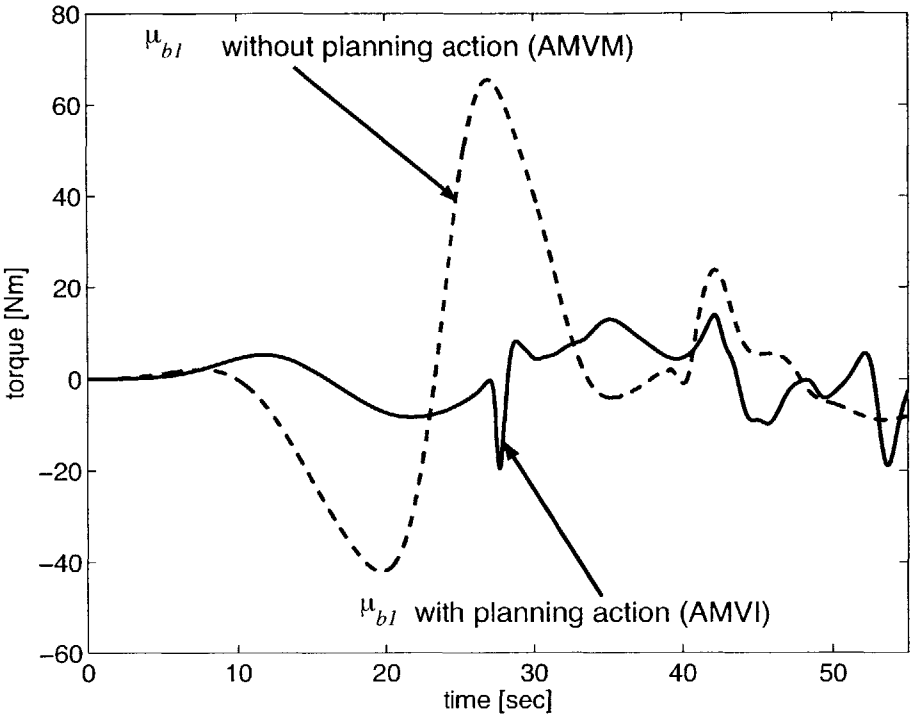

Figure 3.12. Simulation results for the base reaction moment of robot 1 with and without planning action the motion of the robot reaction wheels.

Fig. 3.13 shows simulation results for the vibration deflection of robot 1 base using the AMVI (includes base reaction force control) and the AMVM (does not include base reaction force control). These deflections result from the base reaction forces shown in Fig. 3.11. When robots use the AMVM architecture, their base reaction forces induce large vibration deflection in the robot base structures. On the other hand, the AMVI architecture regulates successfully the Y component of the robot base reaction forces and keeps the vibration in the LSS within the specifications of Table 3.1.

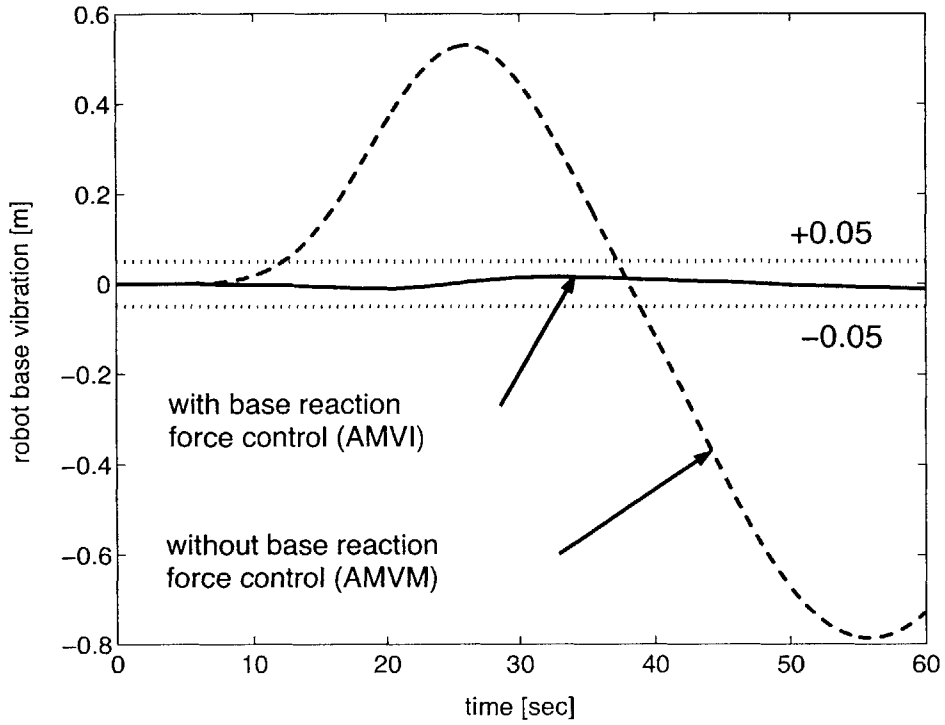

Figure 3.13. Response of robot 1 base structure with and without base reaction force control.

Fig. 3.3 shows that large vibration in the robot base structure can deteriorate significantly the performance of the endpoint force controller. In this case the robots will fail to position the module, Fig. 3.4. On the other hand, Fig 3.14 shows simulation results for the endpoint force of robot 1 using the AMVI architecture. The force tracking performance is good although as good as the result shown in Fig. 2.15, where the robots are mounted on a rigid structure and are controlled using the AMVM architecture. The reason is that after t=30 sec the robots tend to approach the region of undesirable configurations, Section 2.6.4. This can be avoided by increasing the gains of the potential field function term in Eq. 3.12.

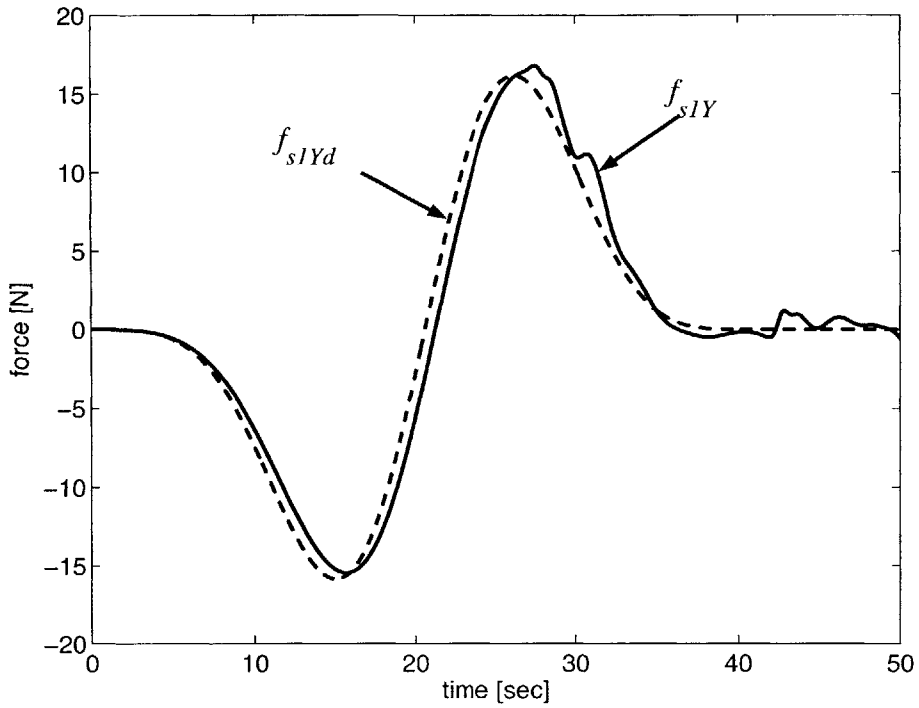

Figure 3.14. Simulation results for the endpoint force of robot 1. Robots use the AMVI planning and control architecture.

Fig 3.15 shows the position response of the beam that corresponds to the force tracking performance of Fig. 3.14. Fig 3.15 shows that the AMVI architecture succeeds in positioning the module within the accuracy specifications of Table 3.1 while exciting low residual vibration in the module and the LSS. The positioning error of the beam CM is kept below 5 cm, whereas the amplitude of residual vibration in the beam end is kept below 2 cm. The application of the AMVI architecture made indeed the robots able to position the beam accurately and with low levels of residual vibration while minimizing the base reaction forces they exert to their base structure.

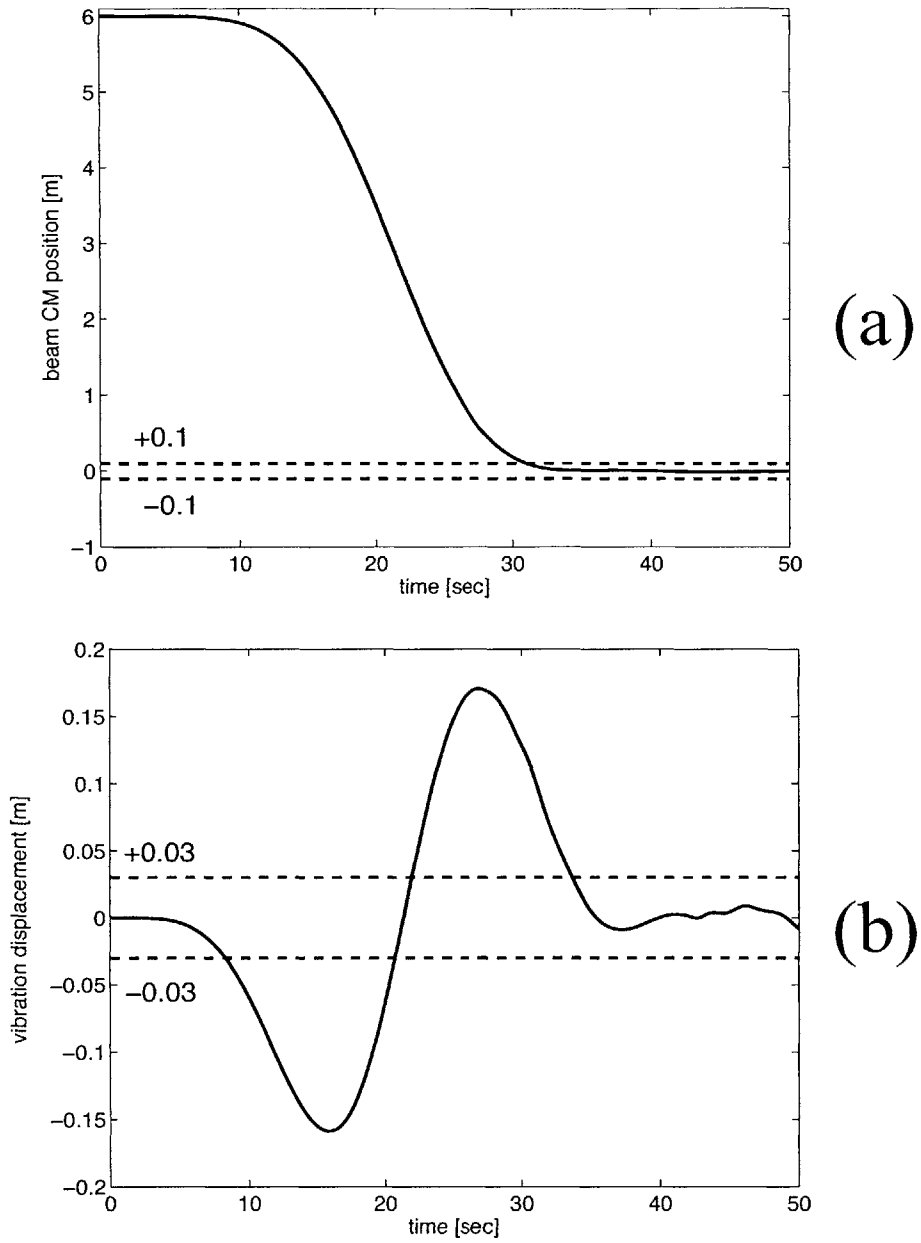

Figure 3.15. Beam CM response (a) and beam left end vibration response (b). Robots use the AMVI planning and control architecture.

Chapter 4
Conclusions and Suggestions for Future Work

4.1 Contributions of this Work

This work has developed a planning and control architecture for the manipulation of large flexible structural modules by a team of space manipulators mounted on the LSS. The key idea of this architecture is that robots can maneuver such delicate structures in a desired way by planning and control the forces that they apply to them.

Chapter 2 presented the planning and control architecture when the compliance of the LSS is not considered. The desired forces that robots need to apply to the module are calculated by a simple force planning algorithm. This algorithm provides smooth sub-optimal force profiles in a computationally efficient way. Robots control the forces they apply to the module cooperatively by using measurements of the forces that they apply to the module. Robots also exploit their redundancy to avoid undesirable configurations. The resulting Architecture for Minimum Vibration Manipulation makes robots able to position the LSS module into its desired pre-assembly position accurately and with low levels of residual vibration.

Chapter 3 expanded the method of Chapter 2 to take into consideration the compliance of the LSS (AMVI). Robots still use the force planning and endpoint force controllers developed in Chapter 2 to control the forces they apply to the module. Furthermore, robots use a base reaction force/moment controller to eliminate the

components of their base reaction forces and moments that induce significant vibration to the LSS. The resulting Architecture for Minimum Vibration Interaction (AMVI) makes robots able to position the LSS module into its desired pre-assembly position accurately and to excite low levels of residual vibration in the module and the LSS.

The ability of space robots to interact successfully with such large and flexible space structures depends strongly on their mechanical design. Robots should be highly redundant, have light links and concentrate their weight in a single middle link (robot body). Robots should have force/torque sensors in their end-effectors to measure and control the forces that they apply to flexible structures. Finally, robots can use reaction wheels to improve their ability to eliminate their base reaction forces and moments.

4.2 Suggestions for Future Work

The manipulation of large flexible structures by robots mounted on compliant base structures is a very challenging task. The planning and control architecture (AMVI) developed in this study will be evaluated experimentally in the new FSRL experimental test-bed, see Appendix B. This work can also be expanded in various directions by eliminating various assumptions that have been used to simplify the analysis.

The AMVI architecture can be applied to more general cases of space robots – large space structures interaction, as shown in Fig. 4.1. The system of interest can consist of many robots of various designs (manipulators or free-flyers) and a number of flexible structures. In such a system some robots interact at the same time with many flexible structures. Similarly, some structures interact with more than one robot. In the AMVI architecture robots perform various tasks to flexible structures (manipulate, damp

vibration, grasp without exerting forces) by planning and control the interaction forces that they apply to the flexible structures. The successful execution of these tasks depends strongly on the effective cooperation between the robots. The performance of the robot team can be enhanced by using global sensing robots to acquire information about the state of the robots and the structures [21]. This information can help robots to compensate the disturbances of their compliant base structures, localize themselves and avoid collisions.

An important future work direction is the compensation of errors in the knowledge of the module inertial properties. When robots control only the interaction forces that they apply to the structures, they need to have accurate dynamic models for the structures so that they can plan properly the forces they need to exert. Errors and uncertainties in the dynamic models of the space structures can be compensated by adding impedance control actions or by using a guidance loop to re-plan the desired interaction forces.

Another important direction for future work is a deeper study of how the performance of the robots is affected by the compliance of the LSS. In this thesis, it was assumed that initially LSS is at rest, therefore vibration in the LSS can be kept small by exerting small base reaction forces and moments. In reality vibration in the LSS can be significant. Robots should be able to position the module precisely and safely even if their bases have some amount of vibration.

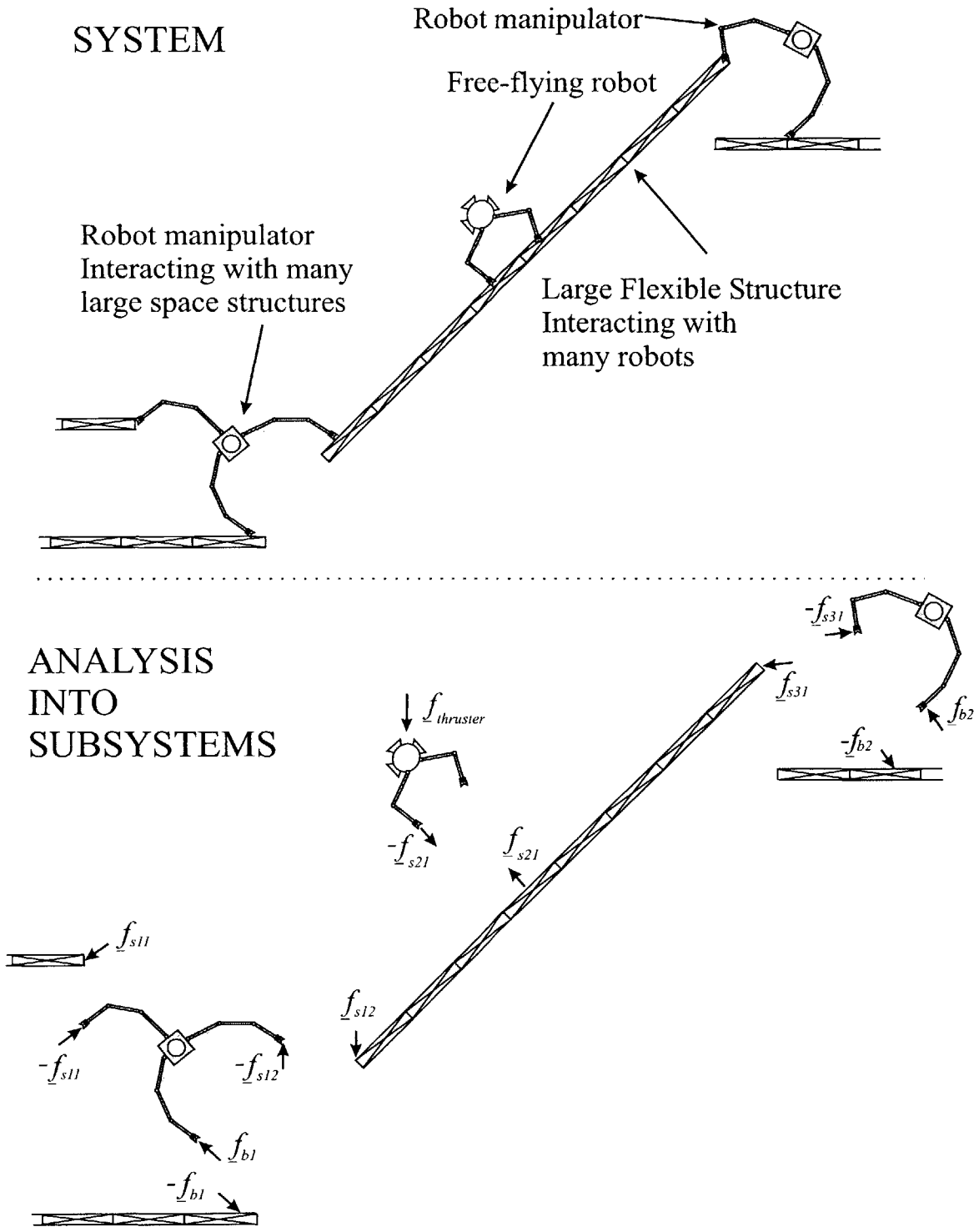

Figure 4.1. Concept for the planning and control of a generic space robots – large flexible structure interaction using the AMVI architecture.

References

[1]: P. Albertos, and A. Sala, *Multivariable Control Systems*, Springer Verlag, 2004.

[2]: M. Balas, "Trends in Large Space Structure Control Theory: Fondest Hopes, Wildest Dreams," *IEEE Transactions on Automatic Control,* vol. 27, no. 3, pp. 522 – 535, June 1982.

[3]: M. Balas, "Feedback Control of Flexible Systems," *IEEE Transactions on Automatic Control,* vol. 23, no. 4, pp. 673 -679, August 1978.

[4]: C. Bendtsen, and P. Thomsen, *Numerical Solution of Differential Algebraic Equations*, Technical Report, Department of Mechanical Engineering, Technical University of Denmark, 1999.

[5]: J. Ben-Asher, J. Burns, and E. Cliff, "Time-Optimal Slewing of Flexible Spacecraft," *AIAA Journal of Guidance, Control and Dynamics,* vol. 15, no. 2, pp. 360 – 367, March – April 1992.

[6]: S. Bhat, and D. Miu, "Precise Point-to-Point Positioning Control of Flexible Structures," *ASME Journal of Dynamic Systems, Measurement and Control*, vol. 112, no. 4, pp. 667-674, December 1990.

[7]: P. Chiacchio, and S. Chiaverini, *Complex Robotic Systems*, Lecture Notes in Control and Information Sciences No. 233, London, Springer Verlag, 1998.

[8]: S. Chiaverini, and B. Siciliano, "The Parallel Approach to Force/Position Control of Robotic Manipulators," *IEEE Transactions on Robotics and Automation,* vol. 9, no. 4, pp. 361-373, August 1993.

[9]: A. Coppa, "Robotic Assembly of Truss Beams for Large Space Structures," *Journal of Spacecraft and Rockets,* vol. 32, no. 4, pp. 680-685, July-August 1995.

[10]: W. Doggert, "Robotic Assembly of Truss Structures for Space Systems and Future Research Plans," *In Proc. IEEE Aerospace Conf. 2002*, March 2002, vol. 7, pp. 3584 – 3598.

[11]: C. Dohrman, et all, *Flexible Robot Dynamics and Controls*, Kluwer Academic Publishers, 2001.

[12]: W. Gawronski, *Dynamics and Control of Structures; A Modal Approach*, Springer Verlag, 1998.

[13]: B. Gordon, S. Liu, and H. Asada, "State Space Modeling of Differential-Algebraic Systems Using Singularly Perturbed Sliding Manifolds," *Proceedings of the ASME Dynamic Systems and Control Division,* vol. 67, pp. 537 – 544, 1999.

[14]: G. Hirzinger, et all, "Robotics and Mechatronics in Aerospace", *In Proc. Seventh International Workshop on Advanced Motion Control AMC*, Maribor, Slovenia, July 2002.

[15]: N. Hogan, "Impedance Control: An approach to Manipulation, Parts I-III," *ASME Journal of Dynamic Systems, Measurement and Control,* vol. 107, pp. 1-24, 1985.

[16]: D. Hyland, J. Junkins, and R. Longman, "Active Technology for Large Space Structures," *AIAA Journal of Guidance, Control and Dynamics,* vol. 16, no. 5, pp. 801 – 821, September – October 1993.

[17]: Y. Ishijima, D. Tzeranis, and S. Dubowsky, "On-Orbit Maneuvering of Large Space Flexible Structures by Free-Flying Robots," *In Proc. Eighth International Symposium on Artificial Intelligence, Robotics and Automation in Space i-SAIRAS*, Munich, Germany, September 2005.

[18]: O. Khatib, "Real-time Obstacle Avoidance for Manipulators and Mobile Robots," *International Journal of Robotics Research*, vol. 1, no. 1, pp. 90-98, Spring 1986.

[19]: O. Khatib, "Inertial Properties in Robotic Manipulation: An Object-Level Framework," *The International Journal of Robotics Research*, vol. 14, no. 1, pp. 19-36, February 1995.

[20]: R. Licata, et all, "Robotic Assembly of XEUS Mirror Sectors on ISS," *In Proc. Seventh International Symposium on Artificial Intelligence, Robotics and Automation in Space i-SAIRAS*, Nara, Japan, May 2003.

[21]: M. Lichter, and S. Dubowsky, "Shape, Motion, and Parameter Estimation of Flexible Space Structures using Range Images," *In Proc. IEEE International Conference on Robotics and Automation ICRA 2005*, Barcelona, Spain, April 2005, pp. 4487-4492.

[22]: V. Mangalgiri, "Analysis for the Robotic Assembly of Large Flexible Space Structures," *MS Thesis, Department of Mechanical Engineering, Massachusetts Institute of Technology*, 2004.

[23]: N. McClamroch, "Singular Systems of Differential Equations as Dynamic Models for Constrained Robot Systems," *In Proc. IEEE International Conf. on Robotics and Automation ICRA 1986*, April 1986, vol. 3, pp. 21 – 28.

[24]: L. Meirovich, *Methods of Analytical Dynamics*, Dover Publications, 1998.

[25]: S. Moosavian, and E. Papadopoulos, "Multiple Impedance Control for Object Manipulation," *In Proc. International Conference on Intelligent Robots and Systems (IROS '98)*, Victoria, BC, Canada, October 1998.

[26]: Y. Nakamura, *Advanced Robotics; Redundancy and Optimization*, Addison-Wesley Publishing, 1991.

[27]: M. Oda M, and M. Mori, "Stepwise Development of SSPS; JAXA's Current Study Status of the 1GW Class Operational SSPS and Its Precursor," *In Proc. 54th International Astronautical Congress of the International Astronautical Federation,* Bremen, Germany, September 2003.

[28]: M. Raibert, and J. Craig, "Hybrid Position/Force Control of Manipulators," *ASME Journal of Dynamic Systems, Measurement and Control*, vol. 103, pp. 126-133, 1981.

[29]: L. Sciavicco, and B. Siciliano, *Modeling and Control of Robot Manipulators*, Second edition, Springer, 2000.

[30]: K. Senda, et all, "Hardware Experiments of Space Truss Assembly by Autonomous Space Robot," *In Proc. AIAA Guidance, Navigation and Control Conference and Exhibit,* Denver CO, August 2000.

[31]: L. Shampine, M. Reichelt, and J. Kierzenka, "Solving Index-1 DAEs in MATLAB and SIMULINK," *SIAM Review*, vol. 41, no. 3, pp. 538-552, 1999.

[32]: N. Singer, and W. Seering, "Preshaping Command Inputs to Reduce System Vibration," *ASME Journal of Dynamic Systems, Measurement and Control*, vol. 112, pp. 76-82, March 1990.

[33]: T. Singh, "Fuel/Time Optimal Control of the Benchmark Problem," *AIAA Journal of Guidance, Control and Dynamics*, vol. 18, no. 6, pp. 1225 – 1231, November-December 1995.

[34]: W. Singhose, N. Singer, and W. Seering, "Comparison of Command Shaping Methods for Reducing Residual Vibration," *In Proc. Third European Control Conference,* Rome, Italy, 1995, vol. 2, pp. 1126-1131.

[35]: P. Staritz, et all, "Skyworker: A Robot for Assembly, Inspection and Maintenance of Large Scale Orbital Facilities," *In Proc. IEEE International Conf. on Robotics and Automation ICRA 2001*, 2001, vol. 4, pp. 4180-4185.

[36]: J. Stokes, "Analysis of Large Space Structures Assembly; Man/Machine Assembly Analysis," *NASA Center for Aerospace Information, Contractor Report 3751*, December 1983.

[37]: D. Sun, and Y. Liu, "Modeling and Impedance Control of a Two-Manipulator System Handling a Flexible Beam," *ASME Journal of Dynamic Systems, Measurement and Control,* vol. 119, no. 4, pp. 736 – 742, December 1997.

[38]: D. Sun, and Y. Liu, "Position and Force Tracking of a Two-Manipulator System Manipulating a Flexible Beam Payload," *In Proc. IEEE International Conf. on Robotics and Automation ICRA 2001*, 2001, vol. 4, pp. 3483-3488.

[39]: D. Sun, J. Mills, and Y. Liu, "Position Control of Robot Manipulators Manipulating a Flexible Payload," *The International Journal of Robotics Research*, vol. 18, no. 3, pp. 319 – 332, March 1999.

[40]: M. Torres, and S. Dubowsky, "Path Planning for Elastically Constrained Space Manipulator Systems," *In Proc. IEEE International Conf. on Robotics and Automation ICRA 1993*, May 1993, vol. 1, pp. 812-817.

[41]: J. Turner, and J. Junkins, "Optimal Large-Angle Single-Axis Rotational Maneuvers of Flexible Spacecraft," *AIAA Journal of Guidance and Control*, vol. 3, no. 6, pp. 578 – 585, Nov – Dec 1980.

[42]: H. Ueno, et all, "On Control and Planning of a Space Station Robot Walker," *In Proc. IEEE International Conference on Systems Engineering,* Aug, 1990, pp. 220 – 223.

[43]: I. Uzmay, R. Burkan, and H. Sarikaya, "Application of Robust and Adaptive Control Techniques to Cooperative Manipulation," *Control Engineering Practice,* vol. 12, pp. 139 – 148, 2004.

[44]: J. Watson, T. Collins, and H. Bush, "A history of astronaut construction of large space structures at NASA Langley Research Center," *In Proc. 2002 IEEE Aerospace Conference Proceedings,* March 2002, Volume 7, pp. 3569 - 3587.

[45]: W. Whittaker, et all, "Robotics for Assembly, Inspection, and Maintenance of Space Macrofacilities," *In Proc. AIAA Space 2000 Conference*, September 2000.

[46]: K. Yoshida, D. Nenchev, and M. Uchiyama, "Vibration Suppression and Zero Reaction Maneuvers of Flexible Space Structure Mounted Manipulators," *Smart Materials Structures*, vol. 8, no. 6, pp. 847-856, December 1999.

[47]: T. Yoshikawa, *Foundations of Robotics*, MIT Press, 1990.

[48]: Y. Zheng, M. Chen, "Trajectory Planning for Two Manipulators to Deform Flexible Beams," *In Proc. IEEE International Conf. on Robotics and Automation ICRA 1993*, May 1993, pp. 1019 – 1024.

[49]: "European Robotic Arm Brochure," [online document], Available HTTP: http://www.dutchspace.nl

[50]: "Space Solar Power Systems Brochure," [online document], Available HTTP: http://www.ista.jaxa.jp/res/b05/ssps/03.html

Appendix A

Linearized Dynamics of the Robots - Module System

This appendix describes the derivation of a linearized dynamic model of a representative system considered in this study. The system consists of a flexible module that is manipulated by two planar robots that are mounted on a rigid base structure, see Fig. 2.4 in Section 2.3. This linearized dynamic model is used in Chapter 2 to design the endpoint force controller that is used in the AMVM and AMVI architectures.

The module is modeled as an Euler-Bernoulli beam, see Section 2.3. The beam is assumed to be rigid in the X_m direction and flexible in the Y_m direction. Assuming small θ_s, $\dot{\theta}_s$ (the axes X,Y are assumed to coincide with X_m,Y_m), the dynamics of the beam, Eq. 2.9 and 2.10, are described as:

$$\begin{bmatrix} X_1(s) \\ X_2(s) \end{bmatrix} = \underline{G}_{PX} \begin{bmatrix} F_{s1X}(s) \\ F_{s2X}(s) \end{bmatrix} \tag{A.1}$$

$$\begin{bmatrix} Y_1(s) \\ Y_2(s) \end{bmatrix} = \underline{G}_{PY} \begin{bmatrix} F_{s1Y}(s) \\ F_{s2Y}(s) \end{bmatrix} \tag{A.2}$$

where X_i, Y_i are the Laplace transformations of the X and Y component of the position of beam end i (i=1 corresponds to the left end and i=2 to the right end) and $F_{sij}(s)$, $j = X,Y$, is the Laplace transformation of the j component of the force $\underline{f}_{si}$ applied by robot i to the beam.

Each robot is modeled by a constant inertia matrix $\underline{B}_{Ai}$ and a constant viscous damping matrix $\underline{D}_{Ai}$ that are attached to the beam at its corresponding end. The constant matrix $\underline{B}_{Ai}$ used in the derivations is calculated as

$$\underline{B}_{Ai} = \underline{U}(\underline{\theta}_i)\begin{bmatrix}\mu_{\max}(\underline{\theta}_i) & \\ & \mu_{\min}(\underline{\theta}_i)\end{bmatrix}\underline{U}(\underline{\theta}_i)^T \tag{A.3}$$

assuming constant reasonable values of $\mu_{\max}$ and $\mu_{\min}$ (away from singular or undesirable configurations, Section 2.6.4) and that the principle axis of $\underline{B}_{Ai}$ form a 45 deg angle with the inertial axes X, Y. The constant matrix $\underline{D}_{Ai}$ is approximated by the damping matrix $\underline{D}_{Aid}$ that is created by the active damping control law of Eq. 2.32. The matrix $\underline{B}_{Ai}$ is not diagonal. The linearized dynamics of each robot are:

$$\underline{Z}_{Ri}(s)\begin{bmatrix}X_i(s)\\ Y_i(s)\end{bmatrix} = \underline{\Gamma}_i(s) - \underline{F}_{si}(s) = \begin{bmatrix}\Gamma_{iX}(s)\\ \Gamma_{iY}(s)\end{bmatrix} - \begin{bmatrix}F_{siX}(s)\\ F_{siY}(s)\end{bmatrix} \quad , \ \mathrm{i} = 1, 2 \tag{A.4}$$

$$\underline{Z}_{Ri}(s) = \underline{M}_{Ai}s^2 + \underline{D}_{Ai}s = \begin{bmatrix}Z_{RXXi}(s) & Z_{RXYi}(s)\\ Z_{RYXi}(s) & Z_{RYYi}(s)\end{bmatrix} \quad , \ \mathrm{i} = 1, 2 \tag{A.5}$$

where $\underline{\Gamma}_i(s)$ is the Laplace transformation of $\underline{\gamma}_i$. The system inputs are the torques $\underline{\tau}_i$ applied at the robot joints. These are described through $\underline{\Gamma}_i(s)$, because $\underline{\tau}_i$ is calculated from $\underline{\gamma}_i$ through Eq. 2.5. Combining Eq. A.4 with Eq. A.1 and A.2 provides the dynamics between the inputs $\underline{\Gamma}_i(s)$ and the forces applied by robots to the beam $\underline{F}_{si}(s)$:

$$\underline{\Gamma} = \underline{G}_F^{-1}(s)\underline{F}_s \tag{A.6}$$

$$\underline{G}_F^{-1}(s) = \begin{bmatrix}\underline{I} + \underline{Z}_{RXX}(s)\underline{G}_{pX}(s) & \underline{Z}_{RXY}(s)\underline{G}_{pY}(s)\\ \underline{Z}_{RYX}(s)\underline{G}_{pX}(s) & \underline{I} + \underline{Z}_{RYY}(s)\underline{G}_{pY}(s)\end{bmatrix} \tag{A.7}$$

where $\underline{\Gamma} = [\Gamma_{1X} \quad \Gamma_{2X} \quad \Gamma_{1Y} \quad \Gamma_{2Y}]^T$, $\underline{F}_s = [F_{s1X} \quad F_{s2X} \quad F_{s1Y} \quad F_{s2Y}]^T$ and $\underline{Z}_{Rjk}(s)$ is a diagonal matrix whose i-th element is the (j, k) element of $\underline{Z}_{Ri}(s)$. The matrix $\underline{G}_F^{-1}$ is used to calculate the feed-forward action of the robot endpoint force controller, see Section 2.6.3. The matrix $\underline{G}_F^{-1}(s)$ can be written as:

$$\underline{G}_F^{-1}(s) = \frac{1}{N(s)}\underline{D}(s) \tag{A.8}$$

where N(s) is the least common multiple of the denominators of $\underline{G}_F^{-1}(s)$ elements. Then:

$$\underline{F}_s(s) = N(s)\underline{D}^{-1}(s)\underline{\Gamma}(s) \tag{A.9}$$

The matrices $\underline{D}(s)$ and $N(s)\underline{I}$ are written as:

$$\underline{D}(s) = \underline{D}_H \underline{H}(s) + \underline{D}_L \underline{L}(s) \tag{A.10}$$

$$N(s)\underline{I} = \underline{N}_H \underline{H}(s) + \underline{N}_L \underline{L}(s) \tag{A.11}$$

where (m is the order of the polynomial $N(s)$)

$$\underline{H}(s) = s^m \underline{I} \tag{A.12}$$

$$\underline{L}(s) = \begin{bmatrix} \underline{l}(s) & & & \\ & \underline{l}(s) & & \\ & & \underline{l}(s) & \\ & & & \underline{l}(s) \end{bmatrix}, \quad \underline{l}(s) = [s^{m-1} \quad s^{m-2} \quad \ldots \quad s \quad 1] \tag{A.13}$$

By choosing $\underline{v}(s) = \underline{D}^{-1}(s)\underline{\Gamma}(s)$ then:

$$\underline{\Gamma}(s) = \underline{D}(s)\underline{v}(s) = \underline{D}_H \underline{H}(s)\underline{v}(s) + \underline{D}_L \underline{L}(s)\underline{v}(s) \Rightarrow$$

$$\underline{D}_H^{-1}\underline{\Gamma}(s) = \underline{H}(s)\underline{v}(s) + \underline{D}_H^{-1}\underline{D}_L \underline{L}(s)\underline{v}(s) \tag{A.14}$$

Choosing as new state $\underline{x}_F$ so that its Laplace transformation is:

$$\underline{X}_F(s) = \underline{L}(s)\underline{v}(s) = \underline{L}(s)\underline{D}^{-1}(s)\underline{\Gamma}(s) \tag{A.15}$$

the state equations of the system become

$$\dot{\underline{x}}_F = \underline{A}_F \underline{x}_F + \underline{B}_F \underline{\gamma} \tag{A.16}$$

$$\underline{A}_F = \begin{bmatrix} & \underline{I} & & 0 & & 0 & & 0 \\ & 0 & & \underline{I} & & 0 & & 0 \\ \underline{a}_{f1} & 0 & \underline{a}_{f2} & 0 & \underline{a}_{f3} & \underline{I} & \underline{a}_{f4} & 0 \\ & 0 & & 0 & & 0 & & \underline{I} \end{bmatrix}^T \tag{A.17}$$

$$\begin{bmatrix} \underline{a}_{f1} & \underline{a}_{f2} & \underline{a}_{f3} & \underline{a}_{f4} \end{bmatrix} = -\underline{D}_H^{-1} \underline{D}_L \tag{A.18}$$

$$\underline{B}_F = \begin{bmatrix} \underline{b}_{f1} & 0 & \underline{b}_{f2} & 0 & \underline{b}_{f3} & 0 & \underline{b}_{f4} & 0 \end{bmatrix}^T \tag{A.19}$$

$$\begin{bmatrix} \underline{b}_{f1} & \underline{b}_{f2} & \underline{b}_{f3} & \underline{b}_{f4} \end{bmatrix} = -\underline{D}_H^{-1} \tag{A.20}$$

The $\underline{I}$'s and 0's of $\underline{A}_F$ are a result of the definition of $\underline{L}(s)$. The remaining four state equations come from the expression of $\underline{H}(s)\underline{v}(s)$ and again the definition of the $\underline{L}(s)$ matrix. The output equations are found as:

$$\underline{F}_s(s) = N(s)\underline{v}(s) = \underline{N}_H \underline{H}(s)\underline{v}(s) + \underline{N}_L \underline{L}(s)\underline{v}(s) \Rightarrow$$

$$\underline{F}_s(s) = \underline{N}_H \underline{H}(s)\underline{v}(s) + \underline{N}_L \underline{X}_F(s) \Rightarrow$$

$$\underline{F}_s(s) = (\underline{N}_L - \underline{N}_H \underline{D}_H^{-1} \underline{D}_L)\underline{X}_F(s) + \underline{N}_H \underline{D}_H^{-1} \underline{\Gamma}(s)$$

so

$$\underline{f}_s = \underline{C}_F \underline{x}_F + \underline{D}_F \underline{\gamma} \tag{A.21}$$

$$\underline{C}_F = \underline{N}_L - \underline{N}_H \underline{D}_H^{-1} \underline{D}_L \tag{A.22}$$

$$\underline{D}_F = \underline{N}_H \underline{D}_H^{-1} \tag{A.23}$$

It is assumed that $\underline{D}_H$ is invertible. The dynamic model of the system consists of Eq A.16 to Eq. A.23.

Appendix B

Future Experimental Validation

The planning and control architecture developed in this thesis will be validated experimentally in the new FSRL Interactive Robotic Team Microgravity Test-bed. The experimental set-up is currently under design and construction.

Fig. B.1 shows the proposed experiment set-up. Two planar robots manipulate a flexible structure, which consists of two free-floating modules (about 10 kg each) connected by a flexible sheet (about 1m in length). Each module is based on the smooth surface of the granite air-table through three flat air-bearings that operate using CO_2. These bearings almost eliminate the friction between the flexible structure and the table.

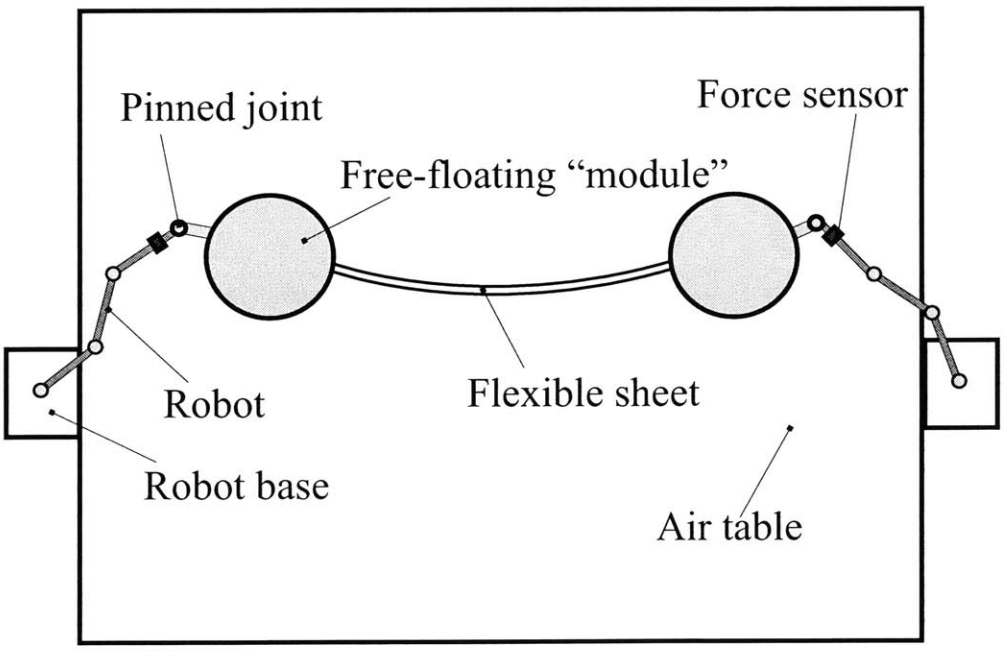

Figure B.1. Schematic of the proposed experiment.

Each robot is firmly attached to a floating module by a pinned joint, has three links (about 15 cm each) and a force sensor at its wrist. This sensor is used to measure and control the forces that the robot applies to the flexible structure. The robots are mounted outside the air-table on rigid or flexible base structures. In the later case, each robot needs an additional force/torque sensor on its base to control its base reaction forces.

The experiment's objective is to apply the planning and control architecture developed in this thesis to maneuver the flexible structure from its initial position to a desired final position accurately and with low levels of residual vibration. The maneuver distance δr is about 50 cm (in the direction normal to the sheet axis). The maneuver duration Δt is about 5 seconds (the period of the structure lowest mode is about 1.5 seconds) and the peak forces between the robot and the flexible structure is about 1.2 N.

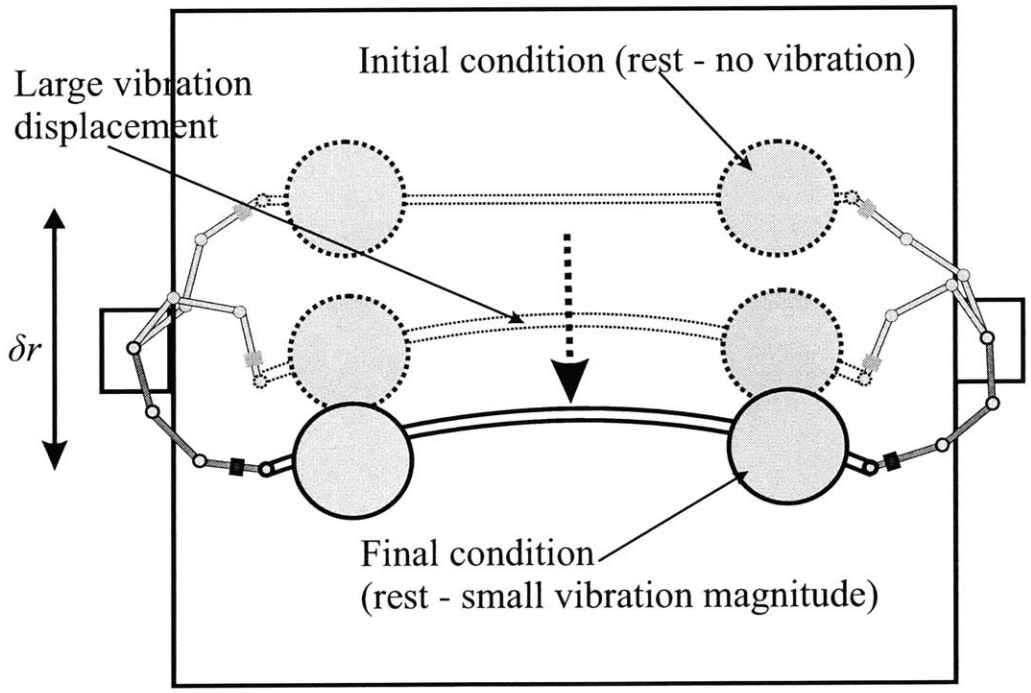

Figure B.2. Snapshots of the proposed experiment.